sustainability

MDPI

Article

A Multi-Objective Optimization Framework for Energy-Efficient Social Housing in Brazil: Balancing Construction Cost and Thermal Comfort Across Diverse Bioclimatic Zones

Rhayssa Padilha Alves [1], Edílson Alves Silva [1], Wanderlei Malaquias Pereira Junior [1], Mayara C. Lima [1], Ed Carlo R. Paiva [1], Emeli Lalesca Aparecida da Guarda [2], Matteo Bodini [3,*] and Leonardo Goliatt [4]

[1] Engineering College, Federal University of Catalão, Catalão 75705-220, GO, Brazil; rhayssa.alves@discente.ufcat.edu.br (R.P.A.); edilson.silva@discente.ufcat.edu.br (E.A.S.); wanderlei_junior@ufcat.edu.br (W.M.P.J.); mayara_cl@discente.ufcat.edu.br (M.C.L.); ed_paiva@ufcat.edu.br (E.C.R.P.)
[2] Department of Architecture and Urban Planning, Federal University of Mato Grosso do Sul, Cidade Universitária, Av. Costa e Silva s/n, Pioneiros, Campo Grande 79070-900, MS, Brazil; emeli.guarda@ufms.br
[3] Department of Pathophysiology and Transplantation, University of Milan, Via Francesco Sforza 35, Zonda Pavilion, 2° Floor, 20122 Milan, Italy
[4] Department of Applied and Computational Mechanics, Federal University of Juiz de Fora, Juiz de Fora 36036-900, MG, Brazil; leonardo.goliatt@ufjf.br
* Correspondence: matteo.bodini@unimi.it

Abstract

Achieving thermal comfort in social housing under variable and changing climates presents a critical challenge for sustainable building design and energy efficiency. This study develops a simulation-based multi-objective optimization framework to support early-stage design of climate-resilient social housing in Brazil, aiming to reduce thermal discomfort and associated mechanical conditioning energy demands. The goal is to identify building envelope configurations that minimize total construction cost while maximizing annual thermal comfort hours, thereby reducing the need for active heating and cooling systems. A reference single-room prototype is simulated in EnergyPlus for five cities representing distinct climatic zones. A wide range of construction alternatives for walls, roofs, slabs, and glazing are evaluated, with costs derived from the national SINAPI database and comfort assessed using the ASHRAE adaptive model based on operative temperature. The optimization, performed with the NSGA-II algorithm (via PyMOO), generates city-specific Pareto fronts that quantify the inherent trade-off between cost and comfort. Results show that optimal solutions range from approximately R$4800 to R$8900 in cost, achieving between 1350 and 3550 annual comfort hours, heavily influenced by local climate. Frequency analysis reveals that wall and roof assemblies are the most influential design variables. The proposed framework provides a transparent, data-driven decision-support tool for defining cost-effective, climate-adapted construction standards, contributing directly to sustainable housing policy, energy poverty reduction, and the development of resilient, low-carbon built environments aligned with the UN Sustainable Development Goals (SDG), particularly SDG 7 (Affordable and Clean Energy), SDG 11 (Sustainable Cities and Communities), and SDG 13 (Climate Action).

Keywords: multi-objective optimization; building performance simulation; energy efficiency; thermal comfort; climate-resilient design; sustainable construction; social housing; building envelope; Pareto frontier; NSGA-II; EnergyPlus; decision-support framework; passive design strategies

Check for updates

Academic Editors: Nuno D. Cortiços, Anna Stefańska and Avi Friedman

Received: 6 February 2026
Revised: 2 April 2026
Accepted: 16 April 2026
Published: 4 May 2026

Copyright: © 2026 by the authors. Licensee MDPI, Basel, Switzerland. This article is an open access article distributed under the terms and conditions of the Creative Commons Attribution (CC BY) license.

1. Introduction

The built environment is facing increasing challenges due to global climate change. The intensification of extreme weather events, such as heat waves and abrupt temperature fluctuations, has placed increasing pressure on the construction sector to rethink design strategies and material choices to mitigate environmental impacts and ensure occupant well-being [1–6]. This issue becomes even more critical given that buildings have long lifespans, exposing them to substantial climate variations throughout their service life [7–9]. As a result, buildings constructed today must be designed to perform effectively not only under current climatic conditions, but also in a future where environmental parameters are expected to shift significantly [10,11]. Moreover, they should aim to reduce the burden of greenhouse gas emissions on both current and future generations [12–14]. In this context, it is essential to develop solutions that balance economic efficiency and thermal performance, especially in increasingly unpredictable climates.

Numerous studies have demonstrated that climate change directly affects the thermal performance of buildings, highlighting the urgent need for adaptive architectural design strategies and the strategic use of appropriate materials [7,15–22]. Building performance simulation tools have become essential instruments for evaluating architectural design alternatives under different climatic conditions [23]. Computational tools such as EnergyPlus [24] allow detailed modelling of heat transfer processes, occupant comfort, and building energy demand, enabling designers to test multiple design strategies before construction [25]. These tools have been widely used to assess the influence of envelope characteristics, building orientation, and material properties on thermal performance and indoor comfort conditions [26,27]. Simulation-based approaches have therefore become increasingly important for supporting evidence-based decision-making in building design, particularly when addressing complex interactions between climate, materials, and occupant comfort [28].

Extreme weather events are becoming more frequent and severe worldwide, underscoring the urgency of climate-resilient building design [29,30]. In Brazil, the city of Araçuaí recorded a historic high of 44.8 °C, the highest temperature ever officially measured in the country [31]. In the United States, 2024 was the warmest year on record for the contiguous states, with several regions experiencing unprecedented heat [32]. In Europe, the highest temperature on record was 48.8 °C in Sicily during the 2021 heatwave, officially validated by the World Meteorological Organization [33]. Meanwhile, in Asia, 2024 brought record-breaking heat, with the average temperature rising 1.04 °C above the 1991–2020 baseline, contributing to widespread and prolonged heatwaves throughout the region [34]. These events highlight the growing climatic variability that buildings must be designed to endure.

Although scientific advancements have significantly improved simulation techniques and introduced new materials, the building industry still faces challenges in integrating thermal performance and energy efficiency measures into contemporary architectural design [35], particularly in developing countries.

In recent years, simulation-based optimization techniques have been increasingly applied to support building design decisions. Multi-objective algorithms allow designers to explore large combinations of design variables and identify solutions that balance competing objectives such as energy consumption, construction cost, and occupant comfort. Among these methods, the Non-dominated Sorting Genetic Algorithm II (NSGA-II) [36] has become one of the most widely adopted approaches due to its ability to generate Pareto-optimal solutions efficiently [37]. Several studies have successfully coupled NSGA-II with building performance simulation tools to optimize building envelope parameters, ventilation strategies, and architectural configurations, demonstrating substantial improvements in energy efficiency and thermal comfort [2,38–41].

This paper aims to investigate the material selection process within architectural design to maximize thermal comfort while minimizing construction costs. The proposed approach seeks to reduce the built environment's exposure to thermal discomfort, thereby contributing to the development of more efficient buildings better adapted to regional climatic conditions.

Objectives and Scope

The present study pursues the following specific objectives: (i) to develop a simulation-based multi-objective optimization framework coupling EnergyPlus building performance simulations with the NSGA-II evolutionary algorithm; (ii) to identify Pareto-optimal building envelope configurations that simultaneously minimize total construction cost and maximize annual thermal comfort hours for social housing; (iii) to evaluate the performance of these configurations across five Brazilian cities representing distinct climatic zones; and (iv) to provide a transparent, data-driven decision-support tool applicable to the early design stages of social housing projects.

The scope of this study is delimited to a single-room residential prototype of 14 m^2, representative of minimum-standard social housing in Brazil. Social housing was selected as the focus of this study due to its high social relevance and its strong connection with national housing policies in Brazil. Despite ongoing government programs to expand housing access, the Brazilian housing deficit remains a persistent challenge, affecting millions of households and disproportionately burdening low-income populations. In this context, improving the environmental performance of social housing is particularly important, as these buildings are typically constructed at large scales and often rely on standardized designs with limited adaptation to local climatic conditions.

Although other passive design strategies, such as shading systems, variations in building orientation, ventilation rates, and adjustments to the window-to-wall ratio, can influence thermal performance [42–44], the analysis focuses exclusively on passive envelope design variables. The decision vector was restricted to components for which standardized unit costs are available in the Brazilian SINAPI cost database [45] and whose thermal properties are characterized in accordance with the Brazilian standard ABNT NBR 15220, thereby ensuring internal consistency of the cost objective function. Thermal comfort is assessed using the ASHRAE adaptive model based on operative temperature, without including active mechanical conditioning systems.

The optimization is conducted independently for each of the five selected cities (Catalão, Curitiba, São Paulo, Belém, and Recife), covering a wide spectrum of Brazilian climatic conditions. Aspects such as multi-room layouts, occupant behavior modeling, life-cycle cost analysis, and future climate scenarios are beyond the scope of this work. A critical discussion of these and other methodological limitations is provided in Section 4, and they are identified as promising directions for future research.

2. Thermal Comfort

The concept of thermal comfort is defined by the American Society of Heating, Refrigeration and Air Conditioning Engineers (ASHRAE) as the state of mind that expresses satisfaction with the surrounding thermal environment [46]. Local thermal discomfort may arise from several factors, including radiant temperature asymmetry caused by hot or cold surfaces, draughts, localized body cooling due to air movement, vertical air temperature differences, and excessively warm or cold floors [47].

From a physical perspective, thermal comfort is achieved when the human body maintains thermal equilibrium with its surroundings. This condition is governed by the balance between metabolic heat production and the heat exchange mechanisms acting between the body and the built environment. When this balance is disrupted, either by

excessive heat gains or insufficient heat dissipation, thermal discomfort emerges regardless of the objectively measured environmental conditions.

In the built environment, thermal control plays a central role in regulating heat exchange processes. Architectural design, material properties, and environmental control strategies directly influence the thermal loads imposed on occupants. Consequently, thermal comfort should not be regarded solely as a physiological phenomenon, but rather as the outcome of a complex interaction between human factors and the thermal behavior of buildings, with direct implications for energy consumption and indoor environmental quality.

2.1. Performance Standards

Concerns regarding thermal comfort predate the consolidation of modern engineering and can be traced back to the nineteenth century. A historically significant milestone was the work History and Art of Warming and Ventilation of Rooms and Buildings, initially published in 1845 by Walter Bernan [48], in which the author already recognized that heating and ventilation should not be treated merely as empirical practices, but as a scientific and technical discipline essential to human comfort and health.

Throughout the early twentieth century, this qualitative understanding evolved toward more systematic and quantitative approaches. Between 1913 and 1923, particularly in the United States, organized efforts emerged to develop objective thermal comfort indices by correlating environmental, physiological, and perceptual variables. These pioneering studies laid the foundation for the formulation of technical criteria and standardized methods to assess indoor thermal conditions.

Since then, thermal comfort research has expanded globally, resulting in the development of a wide range of models, indices, and performance standards. Recent studies emphasize the multidimensional nature of thermal comfort and the importance of human-centered factors. Lin and Zhang [49] showed that psychological conditions can influence thermal perception and acceptable temperature ranges. At the same time, advances in intelligent building operation are enabling adaptive control strategies. Shang et al. [50] demonstrated that reinforcement learning based ventilation control can improve both energy efficiency and indoor air quality.

This progress ultimately led to the consolidation of international and national normative frameworks that guide the design, assessment, and control of thermal environments in buildings, including ISO 7730 [47], ISO 7726 [51], ISO 17772-1 [52], ANSI/ASHRAE Standard 55 [46], EN 16798-1 [53], and, in the Brazilian context, ABNT NBR 15575 [54]. These standards provide technical support to ensure that occupant thermal comfort, building energy efficiency, and indoor environmental quality are simultaneously met.

2.2. Operative Temperature (T_o)

In this study, the concept of operative temperature was adopted to assess thermal comfort within the optimization process. The operative temperature, T_o, represents the uniform temperature of an imaginary environment in which an occupant would exchange the same amount of heat by convection and radiation as in the actual environment. The adaptive thermal comfort model for naturally ventilated spaces was employed, based on the premise that occupants' thermal perception adjusts to prevailing outdoor climatic conditions.

This model applies to naturally ventilated spaces without mechanical air-conditioning, where the prevailing mean outdoor temperature, $t_{pma(out)}$, falls within the range of 10 °C to 33.5 °C (50 °F to 92.3 °F). Two comfort zones are defined, corresponding to 80% and 90% occupant acceptability, each bounded by upper and lower operative temperature limits, as expressed by Equations (1)–(8). Figure 1 presents a graphical representation of the operative temperature and its acceptable ranges.

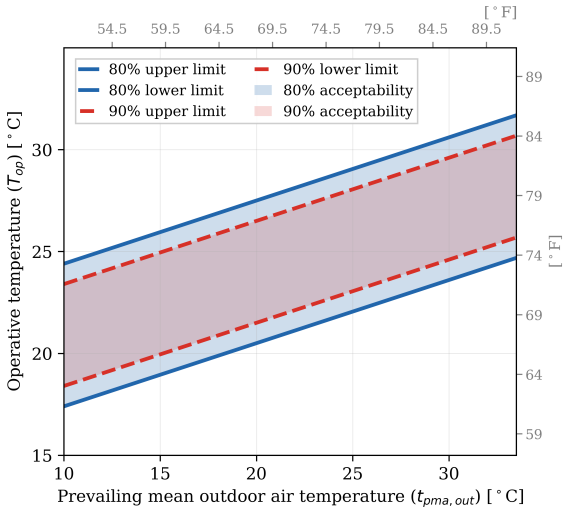


Figure 1. Acceptable operative temperature ranges for naturally conditioned spaces according to ASHRAE Standard 55 (adapted from reference [46]).

The 80% acceptability range defines the operative temperatures within which at least 80% of occupants are expected to find the thermal environment acceptable. The upper limit is given by

$$T_{\text{op,80\%,u}}\,(^{\circ}\text{C}) = 0.31\,t_{\text{pma(out)}} + 21.3 \tag{1}$$

$$T_{\text{op,80\%,u}}\,(^{\circ}\text{F}) = 0.31\,t_{\text{pma(out)}} + 60.5 \tag{2}$$

and the lower limit is expressed as

$$T_{\text{op,80\%,l}}\,(^{\circ}\text{C}) = 0.31\,t_{\text{pma(out)}} + 14.3 \tag{3}$$

$$T_{\text{op,80\%,l}}\,(^{\circ}\text{F}) = 0.31\,t_{\text{pma(out)}} + 47.9 \tag{4}$$

The 90% acceptability range constitutes a more restrictive criterion, establishing the operative temperatures within which at least 90% of occupants are expected to be thermally satisfied. The upper limit is given by

$$T_{\text{op,90\%,u}}\,(^{\circ}\text{C}) = 0.31\,t_{\text{pma(out)}} + 20.3 \tag{5}$$

$$T_{\text{op,90\%,u}}\,(^{\circ}\text{F}) = 0.31\,t_{\text{pma(out)}} + 58.7 \tag{6}$$

and the lower limit is expressed as

$$T_{\text{op,90\%,l}}\,(^{\circ}\text{C}) = 0.31\,t_{\text{pma(out)}} + 15.3 \tag{7}$$

$$T_{\text{op,90\%,l}}\,(^{\circ}\text{F}) = 0.31\,t_{\text{pma(out)}} + 49.7 \tag{8}$$

where $t_{\text{pma(out)}}$ is the prevailing mean outdoor temperature, expressed in the same unit system as the operative temperature limit being computed.

For the assessment of adaptive thermal comfort, an acceptability limit of 80% was adopted, as recommended by ASHRAE 55-2017 for typical applications. This level of acceptability is compatible with the profile of the representative building analyzed in this study.

3. Methodology

This section describes the integrated methodological framework developed to support multi-objective optimization of building envelopes for social housing in Brazilian climatic contexts. As illustrated in Figure 2, the framework operates across five coordinated stages: (1) collection of the two parallel input data streams using climate files (EPW/INMET) and the material–cost database (SINAPI and ABNT NBR 15220); (2) definition of the reference building prototype and its simulation model; (3) coupling of EnergyPlus thermal simulations with the NSGA-II multi-objective optimizer via an automated Python 3.10 workflow, where each candidate envelope solution is evaluated against construction cost (f_1) and annual thermal comfort hours (f_2); (4) aggregation of results into city-specific Pareto fronts; and (5) extraction and analysis of the final outputs, including Pareto-optimal envelope configurations and frequency distributions of selected design variables. The evaluation process within Stage 3 is detailed in Algorithm 1, which defines the sequence of cost computation, model update, simulation, and comfort assessment. This workflow provides a consistent mapping between input data, simulation-based evaluation, and the Pareto-optimal solutions discussed in Section 4.

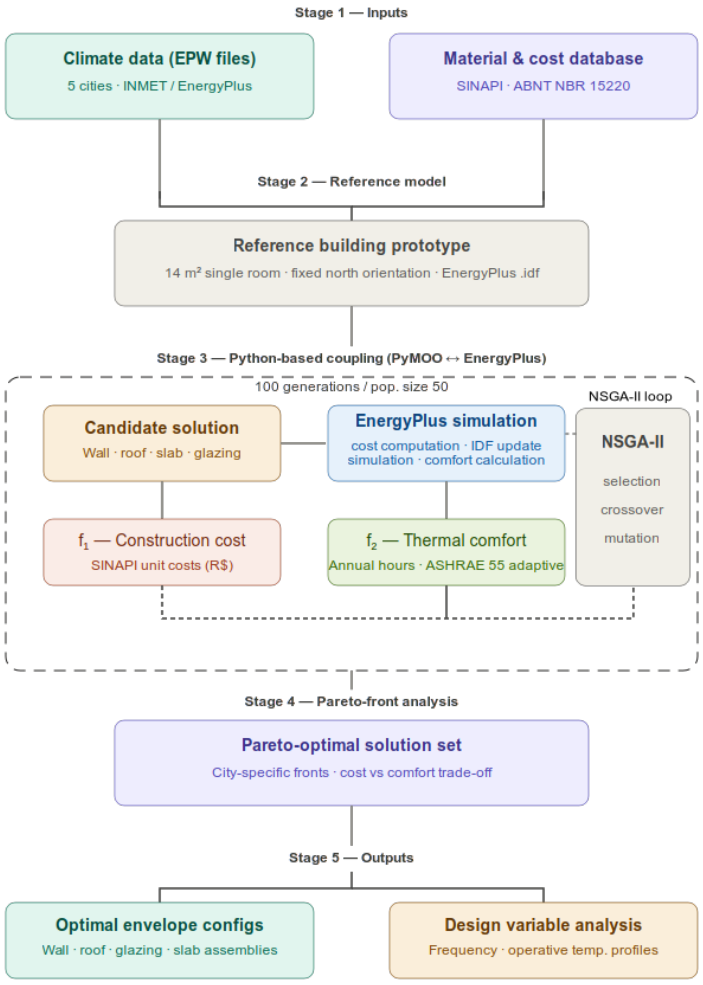


Figure 2. Schematic overview of the methodological workflow. Stage 1 defines the input data, including climate files (EPW/INMET) and material–cost databases (SINAPI and ABNT NBR 15220). Stage 2 establishes the reference building prototype used across all simulations. Stage 3 represents the NSGA-II optimization loop, in which candidate envelope configurations are evaluated in EnergyPlus to compute construction cost (f_1) and annual thermal comfort (f_2). Stage 4 aggregates results into city-specific Pareto fronts. Stage 5 provides the final outputs, including optimal envelope solutions and an analysis of the influence of design variables.

3.1. Reference Building and Climate Data

The framework adopted to evaluate the thermal performance and construction cost of the proposed building prototype focuses on Brazilian conditions, given the country's extensive territory and significant climatic diversity. Figure 3 shows the selected locations, distributed across five distinct Brazilian macro-regions, spanning a diverse spectrum of climatic conditions, consistent with the study's objective of evaluating envelope optimization across diverse environmental contexts. This approach allows the assessment of how the same building configuration performs under distinct environmental conditions, providing insights into the adaptability of compact social housing designs across multiple climates.

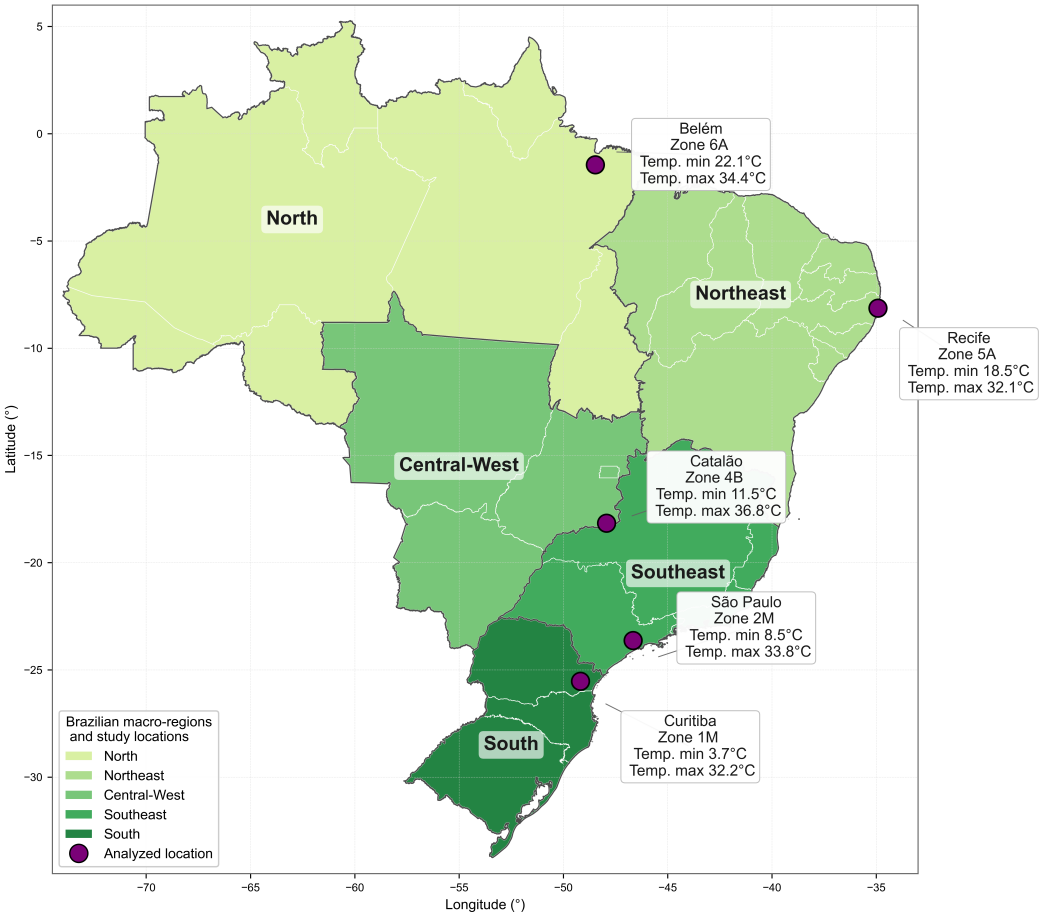


Figure 3. Geographic location of the five Brazilian cities considered in the thermal simulations, shown within the national macro-regional division and each study location together with its corresponding bioclimatic zone. The minimum and maximum temperatures are derived from the EPW weather files used in the analysis.

Thermal performance simulations were conducted using EnergyPlus. Table 1 presents a summary of the assumptions adopted in the simulations, and Table 2 shows the material and associated thermo-physical properties. The weather files in EPW format were obtained from the INMET database, available on the EnergyPlus website (https://energyplus.net/weather) (accessed on 1 April 2026), covering the period from 2001 to 2010, for the cities shown in Table 3. In addition to the weather files, the simulations require an input file (.idf) that contains the building geometry and thermal performance parameters.

These files represent historical climatic conditions and are used as a reference for the optimization of the building envelope. It is important to note that the study does not incorporate future climate change projections. Nevertheless, the proposed approach seeks

to contribute to climate resilience by identifying envelope configurations that maintain adequate thermal performance under the regional climate variability present in Brazil.

Table 1. Simulation assumptions using EnergyPlus.

Aspect	Description	Rationale
Ground contact	Thermal interaction with the ground was considered using standard ground-related properties derived from the climate file.	Standard EnergyPlus ground modeling for realistic heat transfer.
Solar orientation	The building was oriented with the main façade facing north.	Ensures comparability across simulation scenarios.
Occupancy schedule	Residential profile: continuous presence during nighttime hours (10 p.m. to 8 a.m.), with the space remaining unoccupied during daytime hours (8 a.m. to 10 p.m.). Two occupants were considered.	Representative of social housing patterns.
Air infiltration	Not considered in the simulation (rate = 0 ACH).	Focus on envelope optimization; updated per reviewer feedback.
Ventilation	Windows were set to provide natural ventilation when the indoor zone temperature exceeded 19 °C.	Passive strategy emphasis.
Comfort Model	ASHRAE 55 adaptive model (80% acceptability).	Suitable for naturally ventilated spaces without mechanical conditioning.
Simulation period	Full-year simulation using EPW weather files (2001–2010).	Historical baseline; no future climate scenarios included.
Neighboring buildings	Not applicable.	Single prototype room analysis.

The objective of the study is to analyse the influence of envelope design parameters on thermal comfort and construction cost. The EnergyPlus model was not calibrated against field measurements. Instead, the simulation framework was developed using standardized material properties defined in accordance with ABNT NBR 15220 [55] and construction assemblies derived from national technical references. Climatic inputs were obtained from EPW weather files based on INMET meteorological records. Because all design alternatives are evaluated under the same modeling assumptions, the optimization process relies on consistent comparative simulations to identify Pareto-optimal trade-offs between construction cost and thermal comfort. The indoor operative temperature was extracted from the EnergyPlus output variable Zone Operative Temperature (hourly resolution) and compared with the adaptive comfort bounds defined in Equations (1)–(8) at each simulation timestep.

The integration between EnergyPlus and NSGA-II is implemented via an automated and reproducible Python-based framework that evaluates all candidate solutions. This framework programmatically updates the EnergyPlus input file (.idf), executes simulations, extracts hourly operative temperature outputs, computes thermal comfort hours based on the adaptive model, and retrieves cost data from the SINAPI database for each candidate solution. The step-by-step procedure for evaluating each individual in the optimization population is summarized in Algorithm 1.

Algorithm 1: Evaluation of MOO solutions: cost (f_1) and comfort (f_2)

Input: Decision vector encoding parameters $\mathbf{x} = \{\texttt{wall}, \texttt{roof}, \texttt{slab}, \texttt{glazing}\}$

Data: SINAPI Brazilian Government cost database; base .idf file; weather files; simulation routine

Output: Objective pair $(f_1, -f_2)$

Step 1—Build solution: Select wall, roof, slab, and glazing parameters from $\mathbf{x}$

Step 2—Cost (f_1): Query the SINAPI database and compute the total construction cost:

$$f_1 \leftarrow \textsc{CostSINAPI}(\mathbf{x})$$

Step 3—Update model: Update the .idf file with the selected `CONSTRUCTION` parameters

Step 4—Run simulation: Run EnergyPlus using the updated .idf file

Step 5—Comfort (f_2): Compute the annual number of comfort hours:

$$f_2 \leftarrow \textsc{ComfortHours}(\text{results})$$

Step 6—Return to optimizer: Return $(f_1, -f_2)$ so that both objectives are minimized

return $(f_1, -f_2)$

3.2. Material Database and Cost Assessment

The cost considered in the optimization process was defined as the initial investment required for the construction of the building envelope. The cost assessment was based on data from the National System for Research on Construction Costs and Indices (SINAPI), using the reference database for the state of Goiás (GO), December 2024 [45].

To ensure the accuracy of the model, the calculation incorporated both service compositions and material inputs, ensuring the inclusion of costs related to materials, tools, and labor for the main construction systems. A payroll tax-exempt social charges regime was adopted in accordance with current sector practices. The analysis was restricted to the elements that constitute the design variables: walls, roof, raft foundation, and glazing, whose quantities were extracted directly from the reference geometric model. This approach aimed to isolate the economic impact of architectural choices on thermal performance, excluding indirect costs (BDI) and maintenance expenses.

The construction materials considered in this study were selected based on common building practices for social housing and national technical references. The material options were compiled from the VRAC annex, which provides a catalog of thermal properties, and from the Brazilian energy-efficient building design portal Projeteee [56].

For each building component, i.e., walls, floors, roofs, and windows, multiple construction alternatives were defined. Each alternative was characterized by its relevant thermal and physical properties, including thickness, thermal conductivity, density, specific heat capacity, and solar absorptance. All properties were specified in accordance with the procedures and reference values established by ABNT NBR 15220 [57]. The complete material database and the corresponding thermo-physical properties adopted in this study are summarized in Table 2.

Table 2. Material and associated thermo-physical properties.

Material	Roughness	Thickness (m)	Conductivity (W/(m·K))	Density (kg/m^3)	Specific Heat (J/kg·K)	Thermal Abs.	Solar Abs.	Visible Abs.
Cement Mortar 15 mm	MediumRough	0.015	1.15	1800	1000	0.9	0.4	0.4
Cement Mortar 25 mm	MediumRough	0.025	1.15	1800	1000	0.9	0.4	0.4
Cement Mortar 35 mm	MediumRough	0.035	1.15	1800	1000	0.9	0.4	0.4
Gypsum Mortar 5 mm	Smooth	0.005	0.70	1200	840	0.9	0.2	0.2
Gypsum Mortar 8 mm	Smooth	0.008	0.70	1200	840	0.9	0.2	0.2
Gypsum Mortar 10 mm	Smooth	0.010	0.70	1200	840	0.9	0.2	0.2
Ceramic Block 9 cm	MediumRough	0.09	0.90	1600	920	0.95	0.8	0.8
Ceramic Block 12 cm	MediumRough	0.12	0.90	1600	920	0.95	0.8	0.8
Ceramic Block 14 cm	MediumRough	0.14	0.90	1600	920	0.95	0.8	0.8
Concrete Block 9 cm	MediumRough	0.09	1.75	2400	1000	0.95	0.8	0.8
Concrete Block 14 cm	MediumRough	0.14	1.75	2400	1000	0.95	0.8	0.8
Solid Concrete 10 cm	MediumRough	0.10	1.75	2400	1000	0.95	0.8	0.8
Solid Concrete 12 cm	MediumRough	0.12	1.75	2400	1000	0.95	0.8	0.8
White Paint	Smooth	0.002	0.70	1200	840	0.9	0.2	0.2
Concrete Slab Foundation 80 mm	Rough	0.08	1.75	2400	1000	0.8	0.7	0.7
Concrete Slab Foundation 90 mm	Rough	0.09	1.75	2400	1000	0.8	0.7	0.7
Concrete Slab Foundation 100 mm	Rough	0.10	1.75	2400	1000	0.8	0.7	0.7
Concrete Slab Foundation 110 mm	Rough	0.11	1.75	2400	1000	0.8	0.7	0.7
Concrete Slab Foundation 120 mm	Rough	0.12	1.75	2400	1000	0.8	0.7	0.7
Ceramic Tile Flooring 10 mm	Smooth	0.01	0.90	1600	920	0.3	0.4	0.4
Wood Door	MediumSmooth	0.035	0.12	608	230	0.90	0.60	0.60
Solid Slab 100 mm	Rough	0.10	1.75	2400	1000	0.8	0.7	0.7
Ceramic Precast Slab 120 mm	Rough	0.12	0.90	1600	920	0.95	0.8	0.8
EPS Precast Slab 120 mm	Smooth	0.12	0.04	15	1420	0.1	0.1	0.1
PVC Ceiling 10 mm	Smooth	0.01	0.20	1400	100	0.9	0.3	0.3
Gypsum Ceiling 30 mm	Smooth	0.03	0.35	1000	840	0.1	0.1	0.1
Fiber Cement Tile 80 mm	MediumSmooth	0.08	0.65	1700	840	0.95	0.8	0.8
Ceramic Tile Roof 10 mm	MediumSmooth	0.01	0.90	1600	920	0.95	0.8	0.8
Metallic Tile Roof	Smooth	0.01	55.00	7800	460	0.25	0.25	0.25
Polystyrene (EPS) 40 mm	Smooth	0.04	0.04	15	1420	0.1	0.1	0.1
Polyurethane (PU)	Smooth	0.04	0.03	400	1670	0.9	0.5	0.5

Based on the material properties reported in Table 2, a set of construction assemblies was defined encompassing walls, roofs, slabs-on-grade, and glazing systems. The complete description of these assemblies, together with their corresponding cost data, is provided in Appendix A (Tables A1–A4), where they are presented as the discrete construction options evaluated in the simulations and optimization procedures.

Although a purely combinatorial approach would yield up to 41,160 theoretical configurations, a structured selection strategy was applied to ensure physical feasibility, compliance with established constructive practices, and representativeness of social housing typologies. As a result, the final dataset comprises 98 wall assemblies, 14 roof configurations, 4 window glazing types, and 7 slab-on-grade solutions.

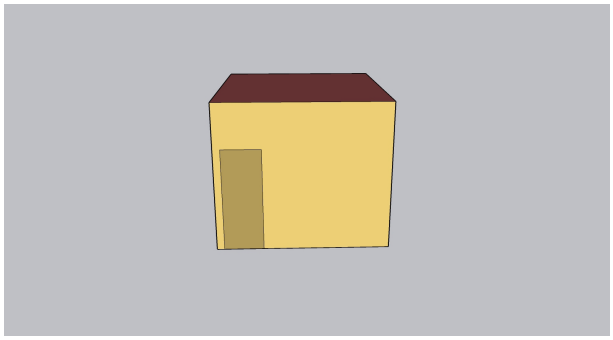
This reduced yet comprehensive set of construction options preserves the diversity of thermophysical characteristics while enabling a robust and computationally efficient assessment of the influence of envelope and foundation systems on building thermal performance.

The case study was based on a representative housing unit environment, referred to as `ROOM` in the simulation model. Table 3 presents the climatic characteristics of the weather files used. A total of five cities were selected for the computational analysis. This selection aimed to evaluate the performance of the same building configuration under different climatic conditions.

Table 3. Information on the cities used in the thermal analysis.

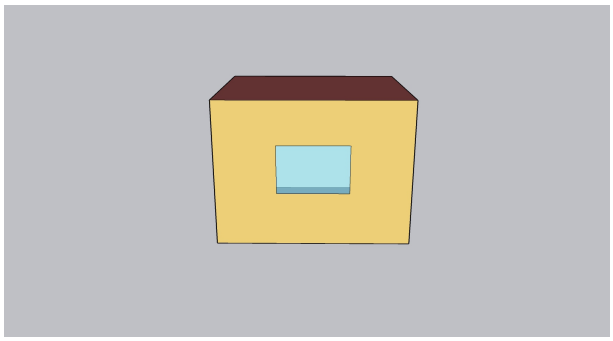
File	City	Lat. (°)	Long. (°)	Alt. (m)	Zone	T_{max} (°C)	T_{min} (°C)	Region
clima_001.epw	Catalão	−18.16	−47.93	890	4B	36.8	11.5	Central-West
clima_002.epw	Curitiba	−25.53	−49.18	910.7	1M	32.2	3.7	South
clima_003.epw	São Paulo	−23.63	−46.66	801.9	2M	33.8	8.5	Southeast
clima_004.epw	Belém	−1.45	−48.47	25.5	6A	34.4	22.1	North
clima_005.epw	Recife	−8.13	−34.92	10.1	5A	32.1	18.5	Northeast

The reference housing model represents a typical single room with internal dimensions of 3.50 m × 4.00 m, resulting in a usable floor area of 14 m^2, in accordance with minimum social housing standards. The room includes an external door with an area of 1.68 m^2 and a window with an area of 1.5 m^2. The architectural façades are shown in Figure 4, and the flat roof has a total area of 14 m^2.

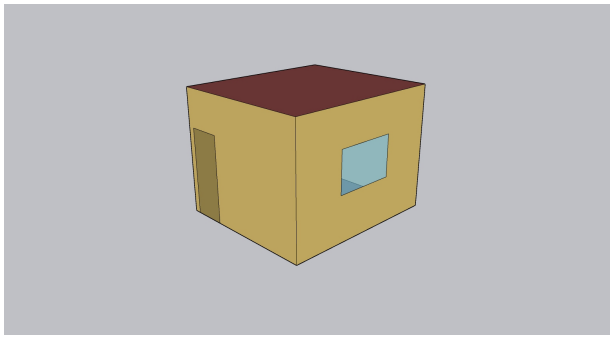


(**a**)

Figure 4. *Cont.*



(**b**)



(**c**)

Figure 4. Prototype building model developed in the SketchUp framework. (**a**) Front view; (**b**) Side view; (**c**) Perspective. The model elements are color-coded as follows: yellow for walls, light blue for windows, dark yellow for the door, and brown for the roof.

3.3. Multi-Objective Building Performance Optimization

Building Performance Optimization (BPO) [58] has become a central strategy in contemporary architectural and building design, aiming to identify solutions that simultaneously enhance energy efficiency, thermal comfort, and economic performance. Traditional parametric simulation approaches typically assess the influence of individual design variables through iterative trial-and-error procedures. However, such approaches are often limited when dealing with highly nonlinear building systems and interacting design parameters, resulting in a restricted exploration of the solution space.

In contrast, simulation-based optimization frameworks integrate Building Performance Simulation (BPS) with computational optimization algorithms, enabling the systematic exploration of a large and complex design space. These methods explicitly account for multiple, often conflicting, performance objectives and allow designers and engineers to identify optimal or near-optimal trade-off solutions that would be difficult to achieve through manual exploration. As a result, BPO provides a more rigorous, automated decision-support framework that supports informed design choices across competing performance criteria [59].

In this study, the Non-dominated Sorting Genetic Algorithm II (NSGA-II) was adopted as the multi-objective optimization technique to support the building performance optimization process. NSGA-II is a well-established evolutionary algorithm for solving multi-objective problems with nonlinear relationships and conflicting objectives, such as minimizing construction costs while maximizing thermal comfort.

The algorithm evolves a population of candidate solutions over successive generations using genetic operators such as selection, crossover, and mutation. Its effectiveness is primarily due to three key mechanisms: fast non-dominated sorting for solution ranking, crowding-distance estimation to preserve population diversity, and elitism to retain high-quality solutions. These features make NSGA-II particularly suitable for architectural and

building design applications, where trade-offs between performance criteria are inherent, and the search space is highly complex.

The optimization framework was implemented using the open-source Python library PyMOO [60], which provides a flexible and extensible environment for multi-objective evolutionary algorithms, including a robust implementation of NSGA-II. PyMOO was coupled with building performance simulations to evaluate each candidate design based on its thermal and economic performance. This integrated workflow enabled the construction of a Pareto-optimal solution set, offering designers a diverse range of optimal trade-off alternatives for informed decision-making.

Table 4 presents the main configuration parameters adopted for the NSGA-II algorithm in this study. The selected values were defined based on preliminary sensitivity analyses and empirical recommendations from the literature, aiming to ensure an adequate balance between convergence, solution diversity, and computational efficiency. These parameters may be further refined in future calibration or scalability assessments.

Table 4. NSGA-II algorithm configuration parameters.

Parameter	Adopted Value
Population size (N)	50
Number of generations	100
Crossover probability (p_c)	0.9
Mutation probability (p_m)	0.2
Selection method	Binary tournament
Crossover method	Simulated Binary Crossover (SBX)
Mutation method	Polynomial Mutation

The optimization problem was formulated to simultaneously minimize two objective functions: the total construction cost (f_1) and the inverse of the thermal comfort indicator ($-f_2$), thereby casting the maximization of thermal comfort hours as a minimization problem. Each individual in the population represents a discrete combination of construction assemblies, enabling the evolutionary process to systematically explore trade-offs between economic performance and thermal comfort.

Since no active mechanical conditioning system was included in the simulation model, annual cooling and heating energy consumption cannot be directly obtained as simulation outputs. Annual thermal comfort hours, therefore, serve as a proxy indicator of reduced mechanical energy demand, as each additional comfort hour represents a period during which active conditioning would not be required to maintain acceptable indoor conditions.

4. Results and Discussion

This section presents the results of the multi-objective optimization process and the subsequent analysis of the solutions located on the resulting Pareto frontier. Section 4.1 discusses the optimized solutions obtained for each of the five cities considered in this study. All results presented are derived directly from the methodological framework described in Section 3, particularly the discrete design space and NSGA-II optimization procedure.

4.1. Optimized Solutions

Figure 5 illustrates the Pareto front obtained for the five analyzed cities. The results indicate that the total construction cost varies approximately between R$ 4800 and R$ 8900, while the total annual thermal comfort ranges from about 1350 to 3550 h.

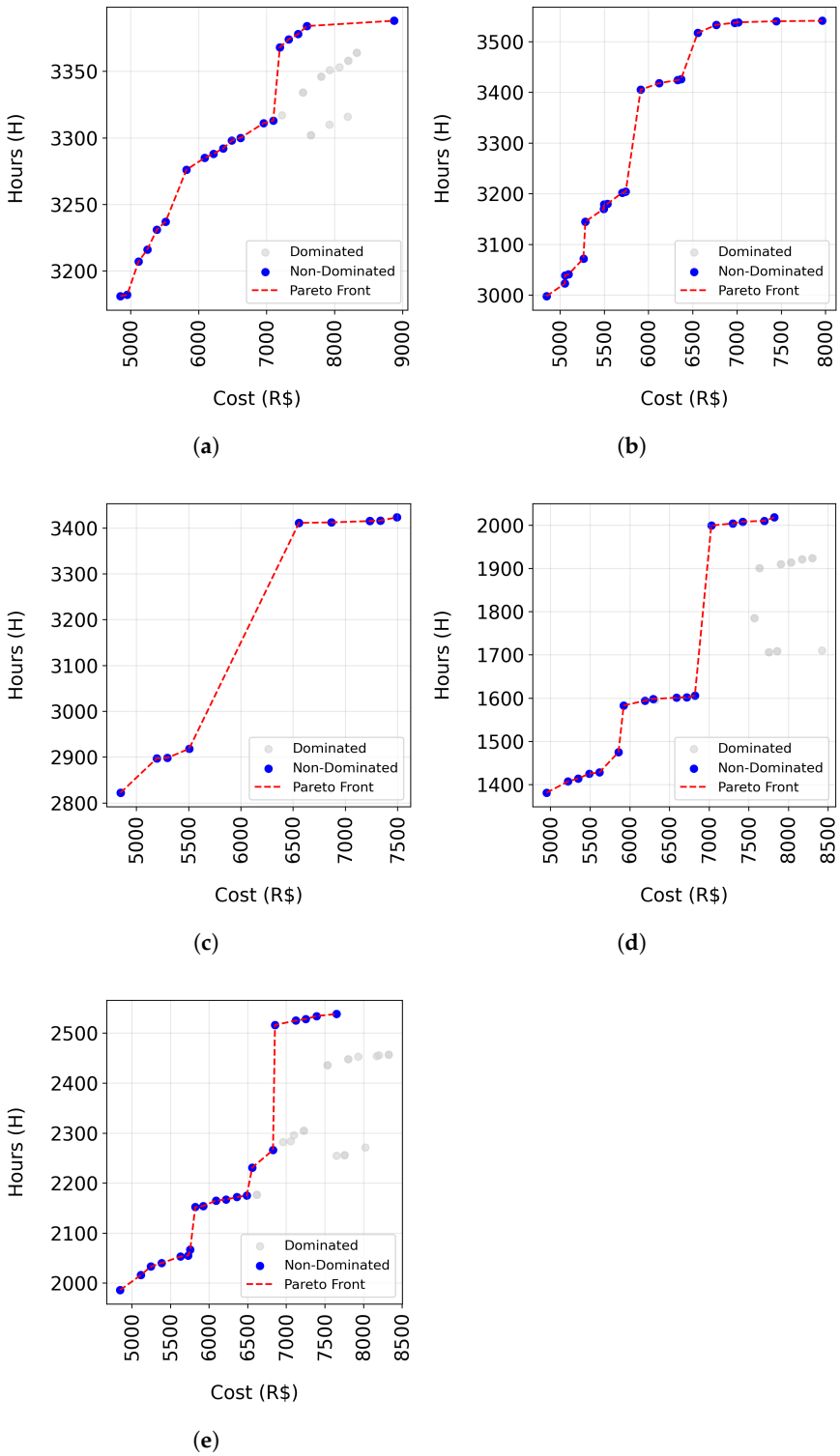


Figure 5. Pareto front of the analyzed cities. (**a**) Catalão; (**b**) Belém; (**c**) Recife; (**d**) Curitiba; (**e**) São Paulo.

Based on Figure 5, the highest construction cost was observed for Catalão, reaching approximately R$8900. Conversely, the minimum-cost solutions were identical across Catalão, Belém, Recife, and São Paulo, all with a minimum value close to R$4800. Table 5 summarizes the total percentage of thermal comfort hours for the corresponding cities.

Table 5. Thermal comfort and cost results for the analyzed cities.

City	Solution	% Comfort	% Discomfort	Cost (R$)
Catalão	Higher-cost	92.85	7.15	8873.48
	Lower-cost	87.17	12.83	4848.46
Belém	Higher-cost	97.04	2.96	7962.10
	Lower-cost	82.16	17.84	4848.46
Recife	Higher-cost	93.80	6.20	7492.53
	Lower-cost	77.34	22.66	4848.46
Curitiba	Higher-cost	55.30	44.70	7823.16
	Lower-cost	37.85	62.15	4950.33
São Paulo	Higher-cost	69.55	30.45	7649.61
	Lower-cost	54.43	45.57	4848.46

The results obtained from the optimization process for the reference housing model reveal significant differences in the constructive combinations selected for each analyzed city, reflecting both the thermal strategies adopted and the total costs of the solutions.

Table 6 presents the detailed envelope configurations for the Pareto-optimal solutions evaluated across Brazilian cities, as referenced in Table 5.

Table 6. Representative Pareto-optimal envelope assemblies from multi-objective optimization across Brazilian cities. Solutions are ranked by construction cost (R$) and thermal discomfort hours (lower is better). Descriptions follow EnergyPlus layer notation (outer to inner).

City	Type	Cost (R$)	Disc. Hrs	Wall	Slab-on-Grade Foundation	Glazing	Roof
Catalão	Highest cost	4907.36	3388	White Paint, 30 mm Cement Mortar, 14 cm Concrete Block, 30 mm Cement Mortar, White Paint	70 mm Concrete Raft Foundation	3 mm Clear Single Glazing	Precast ceramic slab 12 cm, Air chamber 5.0 cm, Metal tile with polystyrene 4 cm
	Lowest cost	3138.93	3181	White Paint, 15 mm Cement Mortar, 14 cm Ceramic Block, 15 mm Cement Mortar, White Paint	70 mm Concrete Raft Foundation	3 mm Clear Single Glazing	PVC ceiling 1 cm, Air chamber 5.0 cm, Ceramic tile 1 cm
Belém	Lowest cost	3138.93	2998	White Paint, 15 mm Cement Mortar, 14 cm Ceramic Block, 15 mm Cement Mortar, White Paint	70 mm Concrete Raft Foundation	3 mm Clear Single Glazing	PVC ceiling 1 cm, Air chamber 5.0 cm, Ceramic tile 1 cm
	Highest cost	4847.51	3541	White Paint, 10 cm Solid Concrete, White Paint	70 mm Concrete Raft Foundation	8 mm Clear Laminated Glazing	Solid slab 10 cm, Air chamber 5.0 cm, Ceramic tile 1 cm
Curitiba	Lowest cost	3138.93	1381	White Paint, 15 mm Cement Mortar, 14 cm Ceramic Block, 15 mm Cement Mortar, White Paint	80 mm Concrete Raft Foundation	3 mm Clear Single Glazing	PVC ceiling 1 cm, Air chamber 5.0 cm, Ceramic tile 1 cm
	Highest cost	4907.36	2018	White Paint, 30 mm Cement Mortar, 14 cm Concrete Block, 30 mm Cement Mortar, White Paint	80 mm Concrete Raft Foundation	3 mm Clear Single Glazing	Solid slab 10 cm, Air chamber 5.0 cm, Metal tile with polyurethane 4 cm
São Paulo	Lowest cost	3138.93	1986	White Paint, 15 mm Cement Mortar, 14 cm Ceramic Block, 15 mm Cement Mortar, White Paint	70 mm Concrete Raft Foundation	3 mm Clear Single Glazing	PVC ceiling 1 cm, Air chamber 5.0 cm, Ceramic tile 1 cm
	Highest cost	4907.36	2538	White Paint, 30 mm Cement Mortar, 14 cm Concrete Block, 30 mm Cement Mortar, White Paint	70 mm Concrete Raft Foundation	3 mm Clear Single Glazing	Solid slab 10 cm, Air chamber 5.0 cm, Metal tile with polystyrene EPS 4 cm

Table 6. *Cont.*

City	Type	Cost (R$)	Disc. Hrs	Wall	Slab-on-Grade Foundation	Glazing	Roof
Recife	Lowest cost	3138.93	4848	White Paint, 15 mm Cement Mortar, 14 cm Ceramic Block, 15 mm Cement Mortar, White Paint	70 mm Concrete Raft Foundation	3 mm Clear Single Glazing	PVC ceiling 1 cm, Air chamber 5.0 cm, Ceramic tile 1 cm
	Highest cost	4847.51	7493	White Paint, 10 cm Solid Concrete, White Paint	70 mm Concrete Raft Foundation	8 mm Clear Laminated Glazing	Plaster ceiling 3 cm, Air chamber 5.0 cm, Ceramic tile 1 cm

Figure 6 shows schematic cross-sections of three representative wall assemblies and three representative roof assemblies drawn from the Pareto-optimal solutions. The assemblies illustrate the key design contrasts between the lower-cost and higher-cost solutions and explain how the material choices differ across climatic contexts.

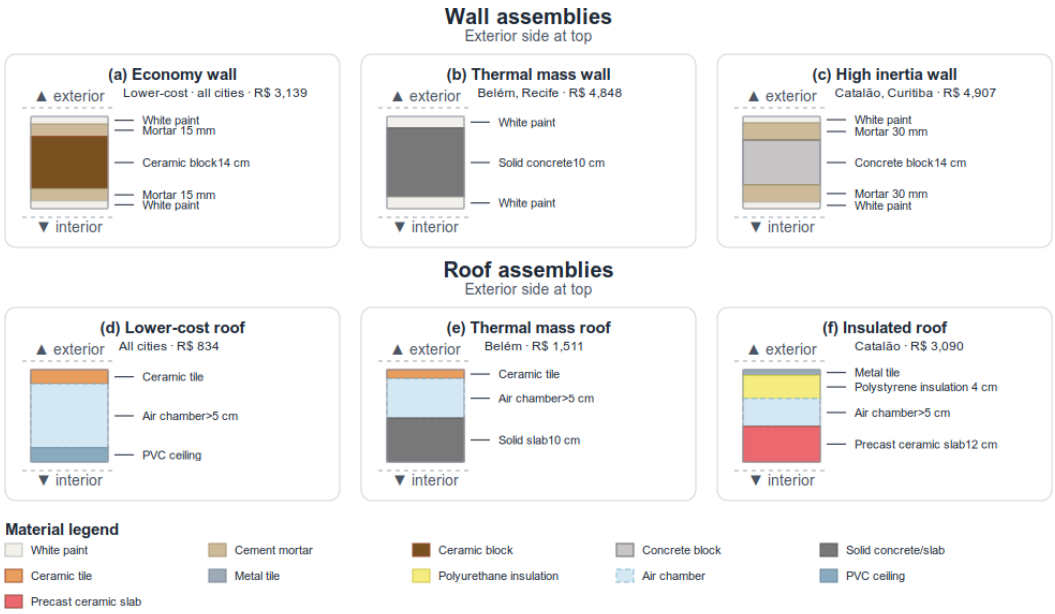


Figure 6. Representative Pareto-optimal envelope assemblies. (**a**–**c**) Wall cross-sections: The economy wall (**a**) is the lower-cost solution common to all cities; the thermal mass wall (**b**) was selected for hot-humid climates (Belém, Recife); and the high inertia wall (**c**) was selected for thermally variable climates (Catalão, Curitiba). (**d**–**f**) Roof cross-sections: The lower-cost roof (**d**) uses a lightweight PVC ceiling below a ventilated ceramic tile; the thermal mass roof (**e**) replaces the PVC ceiling with a 10 cm solid slab; and the insulated roof (**f**) incorporates a metal tile over a precast ceramic slab. Layer thicknesses are shown schematically and not to scale. Costs refer to the individual assembly component only.

For the municipality of Catalão, the highest cost combination was determined by a constructive composition that presented a total value of R$ 8873.48, consisting of a wall formed of white paint, 30 mm cement mortar, a 14 cm concrete block, 30 mm cement mortar, and white paint on the internal surface. The adopted floor system was a 70 mm concrete raft foundation, while the window system used 3 mm clear single glazing. The roof was composed of a 12 cm precast ceramic slab, an air cavity greater than 5 cm, and a metal roof tile with a 4 cm polystyrene layer.

In contrast, the lowest cost solution presented a total value of R$ 4848.46, consisting of a wall with white paint, 15 mm cement mortar, a 14 cm ceramic block, 15 mm cement mortar, white paint, a 70 mm concrete raft foundation, 3 mm clear single glazing, and a roof composed of a 1 cm PVC ceiling, an air cavity greater than 5 cm, and ceramic roof tiles.

For Belém, the lowest cost solution presented the same constructive configuration observed in Catalão, with a wall composed of white paint, 15 mm cement mortar, a 14 cm ceramic block, 15 mm cement mortar, white paint, a 70 mm concrete raft foundation floor, 3 mm clear single glazing, a roof formed by a 1 cm PVC ceiling, an air cavity greater than 5 cm, and ceramic roof tiles, resulting in a total cost of R$ 4848.46. On the other hand, the highest cost solution reached R$ 7962.10, consisting of a 10 cm solid concrete wall with white paint on both faces, a 70 mm concrete raft foundation, a window system with 8 mm laminated clear glass, a roof composed of a 10 cm solid slab, an air cavity greater than 5 cm, and ceramic roof tiles.

In the case of Curitiba, the lowest cost solution presented a total value of R$ 4950.32, composed of a wall with white paint, 15 mm cement mortar, a 14 cm ceramic block, 15 mm cement mortar, white paint, an 80 mm concrete raft foundation floor, a window system with 3 mm clear single glazing, a roof composed of a 1 cm PVC ceiling, an air cavity greater than 5 cm, and ceramic roof tiles. The highest cost combination reached R$ 7823.16 and consisted of a wall with white paint, 30 mm cement mortar, a 14 cm concrete block, 30 mm cement mortar, white paint, an 80 mm concrete raft foundation, 3 mm clear single glazing, a roof composed of a 10 cm solid slab, an air cavity greater than 5 cm, and a metal roof tile with 4 cm polyurethane insulation.

These results demonstrate that different combinations of construction materials can meet the specific climatic conditions of each location, resulting in solutions that balance thermal performance and construction cost.

In terms of thermal comfort, substantial variability is observed among cities. For instance, Recife achieved 77.34% of annual comfort hours, whereas São Paulo reached 54.43%. Similarly, Catalão and Belém achieved 87.17% and 82.16%, respectively. These results demonstrate that, even under comparable cost constraints, thermal performance varies significantly with local climatic conditions, reinforcing the importance of climate-adapted design solutions.

Beyond city-specific analyses, a global assessment was performed by aggregating all optimized construction solutions to identify the most frequently selected decision variables. Specifically, the recurrence of wall systems (x_1), Raft configurations (x_2), window glazing types (x_3), and roof systems (x_4) was analyzed. Figure 7 presents the frequency distribution of these variables, revealing the selection patterns favored by the optimization algorithm.

In the horizontal axis of each graph, the values represent the identification number (ID) of each construction configuration considered in the optimization process rather than a physical measurement unit. Each ID corresponds to a specific design alternative defined in the study. Detailed descriptions of these configurations are provided in Tables A1–A4 of Appendix A.

Among the decision variables, wall systems exhibited the greatest dispersion in construction combinations, indicating a strong sensitivity of the vertical envelope to thermal boundary conditions. The histogram highlights the predominance of combinations 0 and 53, corresponding, respectively, to a 10 cm solid concrete wall with white paint, and to a composite wall consisting of cement plaster (15 mm), ceramic block (14 cm), cement plaster (15 mm), and white paint.

The first solution, characterized by a solid concrete wall, exhibits high thermal mass, providing greater heat storage capacity and attenuating diurnal temperature fluctuations—particularly suitable for regions with high thermal amplitude. In contrast, combination 53 has moderate thermal inertia and lower heat storage capacity, enabling a faster thermal response and lower construction costs.

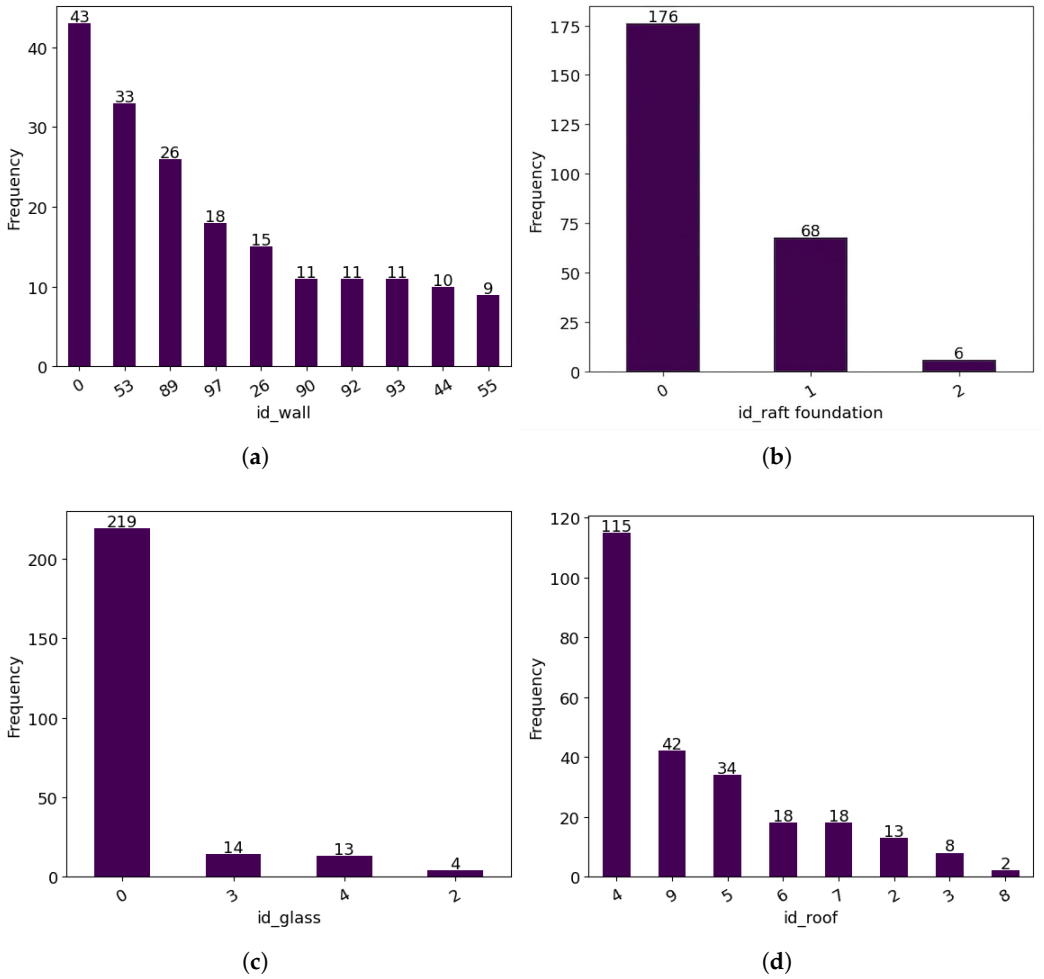


Figure 7. Frequency distribution of selected construction component IDs: (**a**) wall types; (**b**) raft foundations; (**c**) glass types; (**d**) roof configurations.

Raft solutions exhibited low variability, with a strong predominance of combination 0 (70 mm concrete slab) and occasional selection of combination 1 (80 mm slab). This stability indicates that ground-floor systems exerted limited influence on thermal performance, due to reduced heat exchange between the building and the soil.

Window glazing showed an intensely concentrated distribution, with most solutions adopting combination 0, corresponding to 3 mm clear single glazing. Limited occurrences of combination 3, representing 8 mm laminated clear glass, were observed. This predominance suggests that variations in glazing type had a comparatively minor impact on overall thermal performance, especially for small-scale residential buildings with limited window-to-wall ratios.

Roof systems exhibited greater variability compared to other decision variables, although combinations 0 and 9 were dominant. Both configurations consist of a 10 cm solid concrete slab, an air cavity exceeding 5 cm, and a 0.8 cm fiber-cement roofing tile. The primary differences between these solutions lie in the optical properties of the external layer, such as solar reflectance and emissivity, which were adjusted according to local climatic characteristics.

This variability confirms that the roof system plays a central role in controlling the building's thermal performance. In hot, humid climates, solutions favored high-reflectance surfaces and ventilated roof assemblies to reduce direct solar heat gain. Conversely, at high

altitude or in cooler temperatures, configurations with lower thermal transmittance and greater heat-loss resistance were preferred.

4.2. Operative Temperature Assessment

Overall, the dispersion of operative temperature values of the optimized solutions over the 8760 annual simulation hours, as a function of outdoor air temperature, clearly reflects the dominant influence of climatic conditions on building thermal performance. To illustrate these operative behaviors, Figure 8a–d present the lowest- and highest-cost solutions for Belém and Curitiba, cities located in contrasting climatic regions of Brazil.

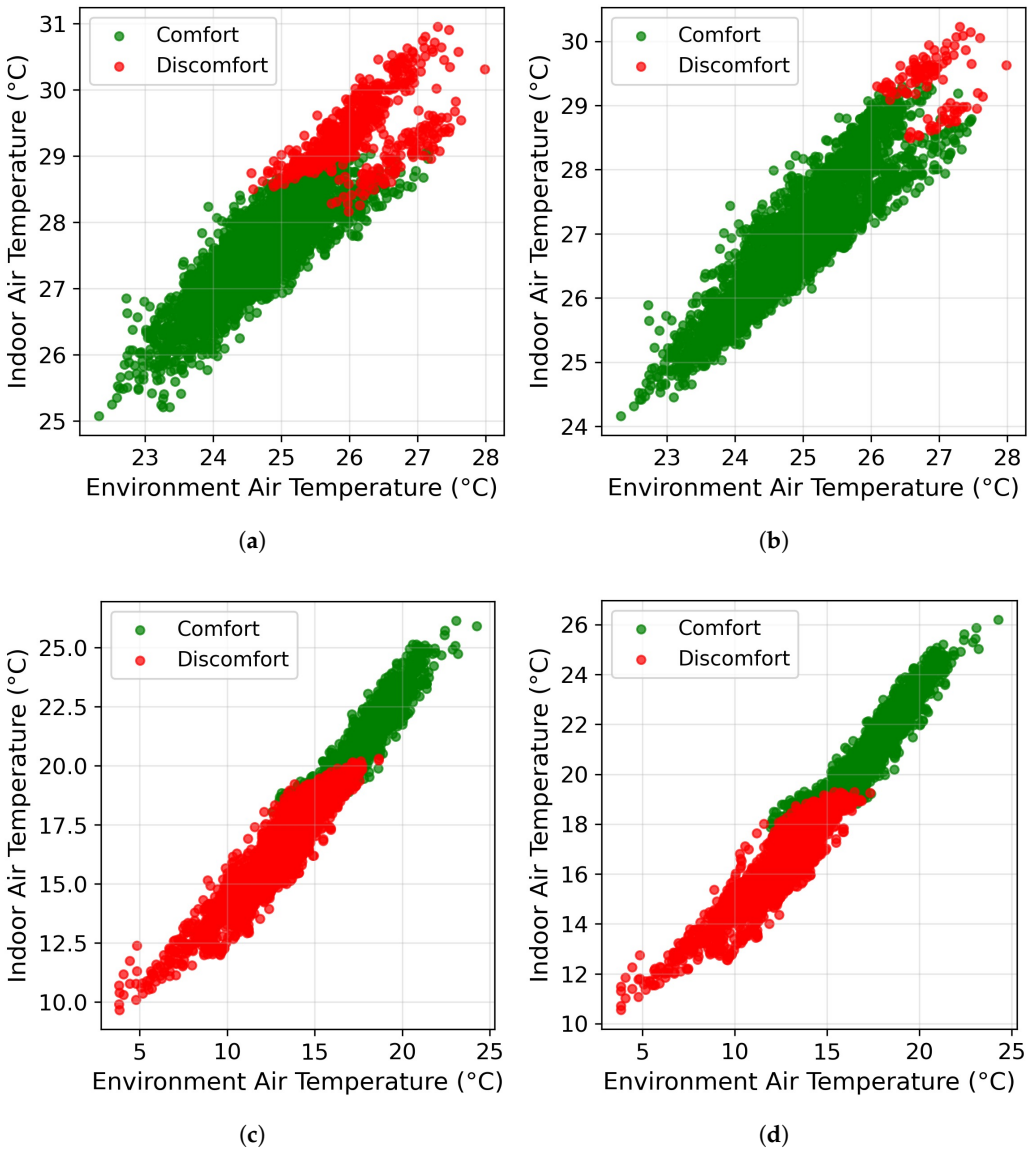


Figure 8. Acceptable operative temperature ranges for naturally conditioned environments for Belém and Curitiba. (**a**) Belém: Lower-cost; (**b**) Belém: Higher-cost; (**c**) Curitiba: Lower-cost; (**d**) Curitiba: Higher-cost.

In Belém, the primary challenge is persistent overheating, resulting in elevated indoor operative temperatures throughout most of the year. In contrast, Curitiba is characterized by predominantly low temperatures, which require greater thermal retention capacity. The corresponding graphs highlight the wide range of internal temperatures and demonstrate how climatic conditions govern indoor thermal behavior.

4.3. Study Limitations

While the proposed framework demonstrates clear utility as a decision-support tool for passive envelope design in social housing, certain methodological limitations must be acknowledged to contextualize the results properly.

The reference building is a highly simplified single-room prototype of 14 m^2, with a fixed north-facing orientation, a standard fixed-occupancy schedule, i.e., nighttime residential presence, and no internal heat gains from occupants or appliances. Empirical evidence indicates that 29% of residents in Brazilian multifamily housing are fully absent during working hours, while 26% remain home all day and 25% return for lunch [61]. In addition, since lower-income occupants rely predominantly on passive adaptive strategies [62,63], the impact of daytime presence on active conditioning demand is partially attenuated for the social housing population studied. Such an abstraction, while appropriate for comparative optimization across climatic zones, does not capture the full thermal complexity of real social housing units, which typically involve multi-room layouts, spatial zoning, diverse occupant behaviors, and variable ventilation patterns.

The fixed solar orientation, in particular, may systematically favor or penalize certain envelope configurations depending on the city's solar path, and results should be interpreted with this constraint in mind. Moreover, the optimization was performed independently for each location, without accounting for multi-zone thermal interactions that would be present in attached or multi-story housing typologies.

Thermal comfort was assessed relying on the ASHRAE 55 adaptive model based on operative temperature, which was selected for its suitability in naturally ventilated spaces. However, the latter model carries inherent applicability boundaries that must be critically acknowledged. First, the model is formally valid only when the prevailing mean outdoor temperature, $t_{pma(out)}$, falls within the range of 10 °C to 33.5 °C. In Belém, where ambient temperatures frequently approach or exceed the upper boundary of this range, the adaptive comfort assessment may be operating near the edge of the model's validity domain, potentially leading to an underestimation of thermal discomfort during peak periods. Second, the adaptive model does not explicitly account for relative humidity, air velocity distribution, variability in clothing insulation, or metabolic rate, all of which are often recognized as determinants of thermal sensation in hot-humid tropical climates. As a result, the comfort hours reported for cities such as Belém and Recife should be interpreted as estimates derived under idealized conditions rather than strict predictions of occupant satisfaction. Future work should consider integrating humidity-adjusted comfort indices, such as the Predicted Mean Vote (PMV) or the Standard Effective Temperature (SET), particularly for the humid tropical climatic zones covered in the study.

The simulations were conducted exclusively using present-day EnergyPlus Weather files (EPW) sourced from the INMET database, which represent historical climatic conditions. No future climate projections under IPCC scenarios (e.g., SSP2-4.5 or SSP5-8.5) were incorporated into the optimization framework. Brazil is projected to experience significant increases in mean temperature [64], more frequent and intense heatwaves [65,66], and altered precipitation patterns over the coming decades [67]. As a consequence, the optimal envelope configurations identified in this study may exhibit reduced thermal performance under future mid- and long-term climatic conditions [68], thereby increasing comfort deficits over their service life. This represents a meaningful limitation of the present analysis and strongly motivates the incorporation of morphed or synthetic future weather files as a priority for subsequent research.

5. Conclusions

This study investigated how selecting construction materials can reduce thermal discomfort in residential buildings, emphasizing performance-based decision-making during the early design stages. By integrating dynamic thermal simulations in EnergyPlus with automated Python workflows, the research demonstrated that material properties and envelope configurations directly influence indoor thermal conditions and annual comfort outcomes.

The results confirm that bioclimatic design principles are not climate-specific prescriptions but a flexible set of strategies that can be adapted to different environmental contexts when grounded in local climatic conditions. Decisions related to envelope composition, particularly walls, roofs, glazing, and surface finishes, were shown to have a direct and significant impact on the number of hours of thermal discomfort.

The analysis further highlighted that improved thermal performance does not necessarily require radical architectural innovation. Instead, the intelligent adaptation of conventional construction systems through optimized combinations of materials, appropriate use of thermal mass and insulation, and climate-responsive surface properties can substantially enhance indoor comfort while maintaining economic feasibility.

Beyond the performance outcomes, the proposed methodology proved effective as a decision-support tool for the design process. The automation of large-scale simulation scenarios enabled systematic, reliable comparisons among construction alternatives, providing actionable insights for performance-oriented design. This approach aligns with performance-based regulatory frameworks and supports more informed, transparent, and technically grounded decision-making in residential projects.

Several directions remain open for future investigation. First, the reference prototype considered here, i.e., a single-room unit of 14 m^2, could be extended to multi-room and full housing-unit layouts to assess how spatial configuration interacts with envelope performance. Second, and most critically, given the limitation highlighted in Section 4, future work should incorporate projected climate data under different IPCC scenarios (e.g., SSP2-4.5 and SSP5-8.5) to evaluate the long-term resilience of the optimized solutions and their adaptability to anticipated climatic shifts. Third, active conditioning strategies, cross-ventilation schedules, and shading devices could be introduced as additional decision variables, broadening the design space beyond passive envelope choices. Future work should also evaluate the sensitivity of Pareto-optimal envelope configurations to diverse occupancy profiles, incorporating schedules representative of households with elderly occupants, children, or home-based workers. Finally, replacing EnergyPlus simulations with surrogate machine learning models, such as gradient boosting regressors or neural networks trained on the existing simulation dataset, could substantially reduce computational overhead, enabling higher-resolution Pareto analyses and broader geographic coverage across Brazilian climatic zones.

Author Contributions: Conceptualization, R.P.A. and W.M.P.J.; methodology, E.C.R.P., E.L.A.d.G., E.L.A.d.G. and W.M.P.J.; software, R.P.A., E.A.S. and M.C.L.; validation, W.M.P.J., L.G., E.L.A.d.G., E.A.S. and E.C.R.P.; formal analysis, R.P.A., E.L.A.d.G., M.B. and E.A.S.; investigation, R.P.A., E.A.S. and E.L.A.d.G.; resources, L.G., E.C.R.P. and M.B.; data curation, R.P.A., M.C.L. and E.C.R.P.; writing—original draft preparation, R.P.A.; writing—review and editing, M.B., W.M.P.J., M.C.L. and L.G.; visualization, R.P.A., E.A.S., L.G. and M.C.L.; supervision, L.G. and W.M.P.J.; project administration, W.M.P.J. and L.G.; funding acquisition, M.B. All authors have read and agreed to the published version of the manuscript.

Funding: This work was supported by the Coordination for the Improvement of Higher Education Personnel (CAPES) under grants Finance Code 001 and 88881.914003/2023-01. LG acknowledges the support of the funding agencies CNPq (grants 307688/2022-4, 409433/2022-5 and 304646/2025-3),

Fapemig (grants APQ-02513-22, APQ-04458-23 and BPD-00083-22), and Finep (grant SOS Equipamentos 2021 AV02 0062/22).

Institutional Review Board Statement: Not applicable.

Informed Consent Statement: Not applicable.

Data Availability Statement: All information required to reproduce the results presented in this study is available from the author WMPJr upon reasonable request.

Conflicts of Interest: The authors declare no known competing financial interests or personal relationships that could have appeared to influence the work reported in this paper.

Appendix A

This appendix provides a detailed description of the construction assemblies and cost information adopted in the simulations. Tables A1–A4 present the complete set of wall, roof, radier, and window glazing configurations derived from the base material properties summarized in Table 2.

For transparency and reproducibility, all cost values reported in the appendix are expressed in Brazilian currency (BRL) and correspond to reference prices commonly adopted in the national construction sector.

Table A1. Wall construction compositions and their costs.

ID	Exterior Paint	Exterior Coating	Block	Interior Coating	Interior Paint	Total Cost (R$)
0	White Paint	-	Solid Concrete 10 cm	-	White Paint	4202.92
1	White Paint	-	Solid Concrete 10 cm	Gypsum Mortar 5 mm	White Paint	4954.01
2	White Paint	-	Solid Concrete 10 cm	Gypsum Mortar 8 mm	White Paint	5155.58
3	White Paint	-	Solid Concrete 10 cm	Gypsum Mortar 10 mm	White Paint	5357.15
4	White Paint	-	Solid Concrete 12 cm	-	White Paint	4847.51
5	White Paint	-	Solid Concrete 12 cm	Gypsum Mortar 5 mm	White Paint	5598.60
6	White Paint	-	Solid Concrete 12 cm	Gypsum Mortar 8 mm	White Paint	5800.17
7	White Paint	-	Solid Concrete 12 cm	Gypsum Mortar 10 mm	White Paint	6001.75
8	White Paint	Cement Mortar 15 mm	Ceramic Block 9 cm	Gypsum Mortar 5 mm	White Paint	4627.21
9	White Paint	Cement Mortar 15 mm	Ceramic Block 9 cm	Gypsum Mortar 8 mm	White Paint	4828.78
10	White Paint	Cement Mortar 15 mm	Ceramic Block 9 cm	Gypsum Mortar 10 mm	White Paint	5030.35
11	White Paint	Cement Mortar 25 mm	Ceramic Block 9 cm	Gypsum Mortar 5 mm	White Paint	4896.55
12	White Paint	Cement Mortar 25 mm	Ceramic Block 9 cm	Gypsum Mortar 8 mm	White Paint	5098.12
13	White Paint	Cement Mortar 25 mm	Ceramic Block 9 cm	Gypsum Mortar 10 mm	White Paint	5299.69
14	White Paint	Cement Mortar 30 mm	Ceramic Block 9 cm	Gypsum Mortar 5 mm	White Paint	5024.80
15	White Paint	Cement Mortar 30 mm	Ceramic Block 9 cm	Gypsum Mortar 8 mm	White Paint	5226.38
16	White Paint	Cement Mortar 30 mm	Ceramic Block 9 cm	Gypsum Mortar 10 mm	White Paint	5427.95
17	White Paint	Cement Mortar 15 mm	Ceramic Block 9 cm	Cement Mortar 15 mm	White Paint	4280.13
18	White Paint	Cement Mortar 15 mm	Ceramic Block 9 cm	Cement Mortar 25 mm	White Paint	4549.47
19	White Paint	Cement Mortar 15 mm	Ceramic Block 9 cm	Cement Mortar 30 mm	White Paint	4677.72
20	White Paint	Cement Mortar 25 mm	Ceramic Block 9 cm	Cement Mortar 15 mm	White Paint	4549.47
21	White Paint	Cement Mortar 25 mm	Ceramic Block 9 cm	Cement Mortar 25 mm	White Paint	4818.80
22	White Paint	Cement Mortar 25 mm	Ceramic Block 9 cm	Cement Mortar 30 mm	White Paint	4947.06
23	White Paint	Cement Mortar 30 mm	Ceramic Block 9 cm	Cement Mortar 15 mm	White Paint	4677.72
24	White Paint	Cement Mortar 30 mm	Ceramic Block 9 cm	Cement Mortar 25 mm	White Paint	4947.06
25	White Paint	Cement Mortar 30 mm	Ceramic Block 9 cm	Cement Mortar 30 mm	White Paint	5075.32
26	White Paint	Cement Mortar 15 mm	Ceramic Block 12 cm	Gypsum Mortar 5 mm	White Paint	3577.81
27	White Paint	Cement Mortar 15 mm	Ceramic Block 12 cm	Gypsum Mortar 8 mm	White Paint	3779.38
28	White Paint	Cement Mortar 15 mm	Ceramic Block 12 cm	Gypsum Mortar 10 mm	White Paint	3980.95
29	White Paint	Cement Mortar 25 mm	Ceramic Block 12 cm	Gypsum Mortar 5 mm	White Paint	3847.15
30	White Paint	Cement Mortar 25 mm	Ceramic Block 12 cm	Gypsum Mortar 8 mm	White Paint	4048.72
31	White Paint	Cement Mortar 25 mm	Ceramic Block 12 cm	Gypsum Mortar 10 mm	White Paint	4250.29
32	White Paint	Cement Mortar 30 mm	Ceramic Block 12 cm	Gypsum Mortar 5 mm	White Paint	3975.40
33	White Paint	Cement Mortar 30 mm	Ceramic Block 12 cm	Gypsum Mortar 8 mm	White Paint	4176.98
34	White Paint	Cement Mortar 30 mm	Ceramic Block 12 cm	Gypsum Mortar 10 mm	White Paint	4378.55
35	White Paint	Cement Mortar 15 mm	Ceramic Block 12 cm	Cement Mortar 15 mm	White Paint	3230.73
36	White Paint	Cement Mortar 15 mm	Ceramic Block 12 cm	Cement Mortar 25 mm	White Paint	3500.07

Table A1. *Cont.*

ID	Exterior Paint	Exterior Coating	Block	Interior Coating	Interior Paint	Total Costs (R$)
37	White Paint	Cement Mortar 15 mm	Ceramic Block 12 cm	Cement Mortar 30 mm	White Paint	3628.32
38	White Paint	Cement Mortar 25 mm	Ceramic Block 12 cm	Cement Mortar 15 mm	White Paint	3500.07
39	White Paint	Cement Mortar 25 mm	Ceramic Block 12 cm	Cement Mortar 25 mm	White Paint	3769.40
40	White Paint	Cement Mortar 25 mm	Ceramic Block 12 cm	Cement Mortar 30 mm	White Paint	3897.66
41	White Paint	Cement Mortar 30 mm	Ceramic Block 12 cm	Cement Mortar 15 mm	White Paint	3628.32
42	White Paint	Cement Mortar 30 mm	Ceramic Block 12 cm	Cement Mortar 25 mm	White Paint	3897.66
43	White Paint	Cement Mortar 30 mm	Ceramic Block 12 cm	Cement Mortar 30 mm	White Paint	4025.92
44	White Paint	Cement Mortar 15 mm	Ceramic Block 14 cm	Gypsum Mortar 5 mm	White Paint	3486.01
45	White Paint	Cement Mortar 15 mm	Ceramic Block 14 cm	Gypsum Mortar 8 mm	White Paint	3687.58
46	White Paint	Cement Mortar 15 mm	Ceramic Block 14 cm	Gypsum Mortar 10 mm	White Paint	3889.15
47	White Paint	Cement Mortar 25 mm	Ceramic Block 14 cm	Gypsum Mortar 5 mm	White Paint	3755.35
48	White Paint	Cement Mortar 25 mm	Ceramic Block 14 cm	Gypsum Mortar 8 mm	White Paint	3956.92
49	White Paint	Cement Mortar 25 mm	Ceramic Block 14 cm	Gypsum Mortar 10 mm	White Paint	4158.49
50	White Paint	Cement Mortar 30 mm	Ceramic Block 14 cm	Gypsum Mortar 5 mm	White Paint	3883.60
51	White Paint	Cement Mortar 30 mm	Ceramic Block 14 cm	Gypsum Mortar 8 mm	White Paint	4085.18
52	White Paint	Cement Mortar 30 mm	Ceramic Block 14 cm	Gypsum Mortar 10 mm	White Paint	4286.75
53	White Paint	Cement Mortar 15 mm	Ceramic Block 14 cm	Cement Mortar 15 mm	White Paint	3138.93
54	White Paint	Cement Mortar 15 mm	Ceramic Block 14 cm	Cement Mortar 25 mm	White Paint	3408.27
55	White Paint	Cement Mortar 15 mm	Ceramic Block 14 cm	Cement Mortar 30 mm	White Paint	3536.52
56	White Paint	Cement Mortar 25 mm	Ceramic Block 14 cm	Cement Mortar 15 mm	White Paint	3408.27
57	White Paint	Cement Mortar 25 mm	Ceramic Block 14 cm	Cement Mortar 25 mm	White Paint	3677.60
58	White Paint	Cement Mortar 25 mm	Ceramic Block 14 cm	Cement Mortar 30 mm	White Paint	3805.86
59	White Paint	Cement Mortar 30 mm	Ceramic Block 14 cm	Cement Mortar 15 mm	White Paint	3536.52
60	White Paint	Cement Mortar 30 mm	Ceramic Block 14 cm	Cement Mortar 25 mm	White Paint	3805.86
61	White Paint	Cement Mortar 30 mm	Ceramic Block 14 cm	Cement Mortar 30 mm	White Paint	3934.12
62	White Paint	Cement Mortar 15 mm	Concrete Block 9 cm	Gypsum Mortar 5 mm	White Paint	3996.31
63	White Paint	Cement Mortar 15 mm	Concrete Block 9 cm	Gypsum Mortar 8 mm	White Paint	4197.88
64	White Paint	Cement Mortar 15 mm	Concrete Block 9 cm	Gypsum Mortar 10 mm	White Paint	4399.45
65	White Paint	Cement Mortar 25 mm	Concrete Block 9 cm	Gypsum Mortar 5 mm	White Paint	4265.65
66	White Paint	Cement Mortar 25 mm	Concrete Block 9 cm	Gypsum Mortar 8 mm	White Paint	4467.22
67	White Paint	Cement Mortar 25 mm	Concrete Block 9 cm	Gypsum Mortar 10 mm	White Paint	4668.79
68	White Paint	Cement Mortar 30 mm	Concrete Block 9 cm	Gypsum Mortar 5 mm	White Paint	4393.90
69	White Paint	Cement Mortar 30 mm	Concrete Block 9 cm	Gypsum Mortar 8 mm	White Paint	4595.48
70	White Paint	Cement Mortar 30 mm	Concrete Block 9 cm	Gypsum Mortar 10 mm	White Paint	4797.05
71	White Paint	Cement Mortar 15 mm	Concrete Block 9 cm	Cement Mortar 15 mm	White Paint	3649.23
72	White Paint	Cement Mortar 15 mm	Concrete Block 9 cm	Cement Mortar 25 mm	White Paint	3918.57
73	White Paint	Cement Mortar 15 mm	Concrete Block 9 cm	Cement Mortar 30 mm	White Paint	4046.82
74	White Paint	Cement Mortar 25 mm	Concrete Block 9 cm	Cement Mortar 15 mm	White Paint	3918.57
75	White Paint	Cement Mortar 25 mm	Concrete Block 9 cm	Cement Mortar 25 mm	White Paint	4187.90
76	White Paint	Cement Mortar 25 mm	Concrete Block 9 cm	Cement Mortar 30 mm	White Paint	4316.16
77	White Paint	Cement Mortar 30 mm	Concrete Block 9 cm	Cement Mortar 15 mm	White Paint	4046.82
78	White Paint	Cement Mortar 30 mm	Concrete Block 9 cm	Cement Mortar 25 mm	White Paint	4316.16
79	White Paint	Cement Mortar 30 mm	Concrete Block 9 cm	Cement Mortar 30 mm	White Paint	4444.42
80	White Paint	Cement Mortar 15 mm	Concrete Block 14 cm	Gypsum Mortar 5 mm	White Paint	4459.25
81	White Paint	Cement Mortar 15 mm	Concrete Block 14 cm	Gypsum Mortar 8 mm	White Paint	4660.82
82	White Paint	Cement Mortar 15 mm	Concrete Block 14 cm	Gypsum Mortar 10 mm	White Paint	4862.39
83	White Paint	Cement Mortar 25 mm	Concrete Block 14 cm	Gypsum Mortar 5 mm	White Paint	4728.59
84	White Paint	Cement Mortar 25 mm	Concrete Block 14 cm	Gypsum Mortar 8 mm	White Paint	4930.16
85	White Paint	Cement Mortar 25 mm	Concrete Block 14 cm	Gypsum Mortar 10 mm	White Paint	5131.73
86	White Paint	Cement Mortar 30 mm	Concrete Block 14 cm	Gypsum Mortar 5 mm	White Paint	4856.84
87	White Paint	Cement Mortar 30 mm	Concrete Block 14 cm	Gypsum Mortar 8 mm	White Paint	5058.42
88	White Paint	Cement Mortar 30 mm	Concrete Block 14 cm	Gypsum Mortar 10 mm	White Paint	5259.99
89	White Paint	Cement Mortar 15 mm	Concrete Block 14 cm	Cement Mortar 15 mm	White Paint	4112.17
90	White Paint	Cement Mortar 15 mm	Concrete Block 14 cm	Cement Mortar 25 mm	White Paint	4381.51
91	White Paint	Cement Mortar 15 mm	Concrete Block 14 cm	Cement Mortar 30 mm	White Paint	4509.76
92	White Paint	Cement Mortar 25 mm	Concrete Block 14 cm	Cement Mortar 15 mm	White Paint	4381.51
93	White Paint	Cement Mortar 25 mm	Concrete Block 14 cm	Cement Mortar 25 mm	White Paint	4650.84
94	White Paint	Cement Mortar 25 mm	Concrete Block 14 cm	Cement Mortar 30 mm	White Paint	4779.10
95	White Paint	Cement Mortar 30 mm	Concrete Block 14 cm	Cement Mortar 15 mm	White Paint	4509.76
96	White Paint	Cement Mortar 30 mm	Concrete Block 14 cm	Cement Mortar 25 mm	White Paint	4779.10
97	White Paint	Cement Mortar 30 mm	Concrete Block 14 cm	Cement Mortar 30 mm	White Paint	4907.36

Table A2. Construction compositions of roofs and their costs.

ID	Combination Description	U (W/m^2·K)	CT (kJ/m^2·K)	α	Cost (R$)
0	Solid slab 10 cm | Air chamber (>5.0 cm) | Fiber cement tile 0.8 cm	2.06	233	0.65	1511.03
1	Precast ceramic slab 12 cm | Air chamber (>5.0 cm) | Ceramic tile 1 cm	1.77	185	0.75	2734.90
2	Precast EPS slab 12 cm | Air chamber (>5.0 cm) | Ceramic tile 1 cm	1.26	150	0.75	2664.90
3	Solid slab 10 cm | Air chamber (>5.0 cm) | Metal tile with polystyrene (EPS) 4 cm	0.68	229	0.30	1866.42
4	PVC ceiling 1 cm | Air chamber (>5.0 cm) | Ceramic tile 1 cm	1.75	21	0.75	833.70
5	Plaster ceiling 3 cm | Air chamber (>5.0 cm) | Ceramic tile 1 cm	1.94	37	0.75	1041.46
6	Solid slab 10 cm | Air chamber (>5.0 cm) | Ceramic tile 1 cm	2.05	238	0.75	1511.03
7	Solid slab 10 cm | Air chamber (>5.0 cm) | Metal tile with polyurethane 4 cm	0.55	230	0.30	1938.10
8	Precast ceramic slab 12 cm | Air chamber (>5.0 cm) | Metal tile with polystyrene 4 cm	0.64	176	0.30	3090.29
9	Precast ceramic slab 12 cm | Air chamber (>5.0 cm) | Metal tile 0.6 cm	1.80	169	0.30	2544.64
10	Precast EPS slab 12 cm | Air chamber (>5.0 cm) | Fiber cement tile 0.8 cm	1.26	145	0.65	3344.34
11	Precast EPS slab 12 cm | Air chamber (>5.0 cm) | Metal tile 0.6 cm	1.80	169	0.30	2474.64
12	Extensive green roof: Solid slab 10 cm | Dry clay soil 10 cm | Vegetation	2.18	363	0.70	2243.36
13	Extensive green roof: Precast slab 12 cm | Dry clay soil 10 cm | Vegetation	1.86	310	0.70	3467.23

Table A3. Concrete raft foundations and their costs.

ID	Raft Thickness (mm)	Cost (R$)
0	70	713.08
1	80	814.95
2	90	916.81
3	100	1018.68
4	110	1120.55
5	120	1222.42

Table A4. Window glazing configurations and their costs.

ID	Glass Thickness (mm)	U-Value (W/m^{2}K)	Solar Factor	Cost (R$)
0	3	5.7	0.87	162.75
1	6	5.7	0.87	263.49
2	8	5.7	0.34	890.48
3	8	5.7	0.39	372.00
4	8	5.7	0.37	410.90

References

1. Barbosa, S.; Alberto, K.C.; Piroozfar, P. Natural daylighting through double skin façades: A review. *Archit. Eng. Des. Manag.* **2025**, *21*, 231–251. [CrossRef]
2. Aburabi'e, M.; Bataineh, K.; Al-Kabaha, Y. Multi objective design optimization of residential buildings: Energy consumption, life cycle cost and thermal discomfort based on NSGA-II. *Innov. Infrastruct. Solut.* **2025**, *10*, 354. [CrossRef]
3. Li, R.; Shari, Z.; Ab Kadir, M.Z.A. A review on multi-objective optimization of building performance-Insights from bibliometric analysis. *Heliyon* **2025**, *11*, e42480. [CrossRef]
4. Hosamo, H.H.; Tingstveit, M.S.; Nielsen, H.K.; Svennevig, P.R.; Svidt, K. Multiobjective optimization of building energy consumption and thermal comfort based on integrated BIM framework with machine learning-NSGA II. *Energy Build.* **2022**, *277*, 112479. [CrossRef]
5. Cruz, A.S.; da Cunha, E.G. The impact of climate change on the thermal-energy performance of the SCIP and ICF wall systems for social housing in Brazil. *Indoor Built Environ.* **2022**, *31*, 838–852. [CrossRef]
6. Garcia, D.R.; Mendes, V.F.; Moraes, C.F.; Cabral, M.M.Q.; Silva, I.B.A.R.; Mendes, J.C. Climate change, thermal comfort, and low-income residences: Insights from post-occupancy evaluations of concrete wall buildings in Brazil. *Sustain. Energy Technol. Assess.* **2026**, *86*, 104847. [CrossRef]
7. Saifudeen, A.; Mani, M. Adaptation of buildings to climate change: An overview. *Front. Built Environ.* **2024**, *10*, 1327747. [CrossRef]

8. Tellache, A.; Lazri, Y.; Laafer, A.; Attia, S. Adaptive Thermal Comfort Assessment in Residential Buildings Under Current and Future Mediterranean Climate Scenarios. *Buildings* **2025**, *15*, 3171. [CrossRef]
9. Soudian, S.; Berardi, U. Impact of future climate scenarios on thermal performance and resilience of building façades: Canadian climate case study. *Build. Environ.* **2025**, *267*, 112245. [CrossRef]
10. Benaddi, F.Z.; Boukhattem, L.; Tabares-Velasco, P.C. Multi-objective optimization of building envelope components based on economic, environmental, and thermal comfort criteria. *Energy Build.* **2024**, *305*, 113909. [CrossRef]
11. Hamdy, M.; Hasan, A.; Siren, K. A multi-stage optimization method for cost-optimal and nearly-zero-energy building solutions in line with the EPBD-recast 2010. *Energy Build.* **2013**, *56*, 189–203. [CrossRef]
12. Pomponi, F.; Moncaster, A. Embodied carbon mitigation and reduction in the built environment–What does the evidence say? *J. Environ. Manag.* **2016**, *181*, 687–700. [CrossRef]
13. Shen, Y.S.; Lin, Y.C.; Cui, S.; Li, Y.; Zhai, X. Crucial factors of the built environment for mitigating carbon emissions. *Sci. Total Environ.* **2022**, *806*, 150864. [CrossRef]
14. Kuittinen, M.; Zernicke, C.; Slabik, S.; Hafner, A. How can carbon be stored in the built environment? A review of potential options. *Archit. Sci. Rev.* **2023**, *66*, 91–107. [CrossRef]
15. Ren, Z. A Literature Review on the Use of Weather Data for Building Thermal Simulations. *Energies* **2025**, *18*, 3653. [CrossRef]
16. Rodrigues, E.; Fernandes, M.S.; Carvalho, D. Future weather generator for building performance research: An open-source morphing tool and an application. *Build. Environ.* **2023**, *233*, 110104. [CrossRef]
17. Zhai, Z.J.; Helman, J.M. Implications of climate changes to building energy and design. *Sustain. Cities Soc.* **2019**, *44*, 511–519. [CrossRef]
18. Rodrigues, E.; Parente, J.; Fernandes, M.S. Building for tomorrow: Analyzing ideal thermal transmittances in the face of climate change in Brazil. *Appl. Energy* **2024**, *355*, 122360. [CrossRef]
19. Bera, M.; Das, S.; Dutta, S.; Nag, P.K.; Roy Choudhury, M. Progress and challenges of bioclimatic design strategies for enhancing building environmental performance: A systematic review. *Smart Sustain. Built Environ.* **2026**, *15*, 948–990. [CrossRef]
20. Shen, P.; Li, Y.; Gao, X.; Chen, S.; Cui, X.; Zhang, Y.; Zheng, X.; Tang, H.; Wang, M. Climate adaptability of building passive strategies to changing future urban climate: A review. *Nexus* **2025**, *2*, 100061. [CrossRef]
21. Lamberti, G.; Contrada, F.; Kindinis, A. Exploring adaptive strategies to cope with climate change: The case study of Le Corbusier's Modern Architecture retrofitting. *Energy Build.* **2024**, *302*, 113756. [CrossRef]
22. Alassaad, K.; Minto, J.; de Wilde, P. Enhancing building thermal performance: A review of phase change material integration. *Energies* **2025**, *18*, 3200. [CrossRef]
23. Cruz, A.S.; López-Guerrero, R.E.; Mendes, V.F.; Mendes, J.C.; Caldas, L.R.; Bastos, L.E.G. A simulation-based procedure for promoting climate-resilient building design in the global south context: The Latin America residential sector perspective. *Energy Build.* **2025**, *353*, 116915. [CrossRef]
24. Crawley, D.B.; Lawrie, L.K.; Winkelmann, F.C.; Buhl, W.F.; Huang, Y.J.; Pedersen, C.O.; Strand, R.K.; Liesen, R.J.; Fisher, D.E.; Witte, M.J.; et al. EnergyPlus: Creating a new-generation building energy simulation program. *Energy Build.* **2001**, *33*, 319–331. [CrossRef]
25. Naeem, A.; Ho, C.O.; Kolderup, E.; Jain, R.K.; Benson, S.; de Chalendar, J. EnergyPlus as a computational engine for commercial building operational digital twins. *Energy Build.* **2025**, *329*, 115257. [CrossRef]
26. Ascione, F.; Bianco, N.; De Masi, R.F.; Mauro, G.M.; Vanoli, G.P. Design of the Building Envelope: A Novel Multi-Objective Approach for the Optimization of Energy Performance and Thermal Comfort. *Sustainability* **2015**, *7*, 10809–10836. [CrossRef]
27. Gabriel, E. Optimization of building envelopes for zero-energy social housing in southern brazilian bioclimatic zones using multi-criteria decision analysis. *Energy Build.* **2026**, *357* , 117119. [CrossRef]
28. Bre, F.; Fachinotti, V.D. A computational multi-objective optimization method to improve energy efficiency and thermal comfort in dwellings. *Energy Build.* **2017**, *154*, 283–294. [CrossRef]
29. da Guarda, E.L.A.; Mizgier, M.O.; Neto, A.H. Impact of climate change on indoor conditions of social residence in Brazil: Assessing occupants' vulnerability. *J. Build. Eng.* **2025**, *113*, 113810. [CrossRef]
30. Villa, S.B.; Bortoli, K.C.R.d.; Oliveira, L.V. Resilient House Evaluation Matrix: Attributes and Quality Indicators for Social Housing. *Buildings* **2025**, *15*, 793. [CrossRef]
31. Pampuch, L.A.; Bueno, P.G.; Reboita, M.S.; Tomaziello, A.C.N.; Nunes, A.M.P.; Cardoso, A.A.; Coelho, C.A.S.; Carpenedo, C.B.; Vasconcelos, F.C., Jr.; Gomes, H.B.; et al. Brazil climate highlights 2023. *Ann. N. Y. Acad. Sci.* **2025**, *1549*, 120–138. [CrossRef]
32. Sandford, C.; Dunn, R.; Killick, R.; Palmer, M.; Titchner, H.; Rayner, N.; Morice, C.; Kendon, M. Global and regional climate in 2024. *Weather* **2025**, *80*, 401–410. [CrossRef]
33. WMO—World Meteorological Organization. *WMO Confirms Verification of New Continental EUROPEAN Temperature Record*; WMO: Geneva, Switzerland, 2024.
34. World Meteorological Organization (WMO). *Rising Temperatures and Extreme Weather Hit Asia Hard*; WMO: Geneva, Switzerland, 2025.

35. Triana, M.A.; Lamberts, R.; Sassi, P. Should we consider climate change for Brazilian social housing? Assessment of energy efficiency adaptation measures. *Energy Build.* **2018**, *158*, 1379–1392. [CrossRef]
36. Deb, K.; Pratap, A.; Agarwal, S.; Meyarivan, T. A fast and elitist multiobjective genetic algorithm: NSGA-II. *IEEE Trans. Evol. Comput.* **2002**, *6*, 182–197. [CrossRef]
37. Abdeen, A.; Mushtaha, E.; Hussien, A.; Ghenai, C.; Maksoud, A.; Belpoliti, V. Simulation-based multi-objective genetic optimization for promoting energy efficiency and thermal comfort in existing buildings of hot climate. *Results Eng.* **2024**, *21*, 101815. [CrossRef]
38. Wei, H.; Jiao, Y.; Wang, Z.; Wang, W.; Zhang, T. Optimal retrofitting scenarios of multi-objective energy-efficient historic building under different national goals integrating energy simulation, reduced order modelling and NSGA-II algorithm. In *Proceedings of the Building Simulation*; Springer: Berlin/Heidelberg, Germany, 2024; Volume 17, pp. 933–954. [CrossRef]
39. Said, M.A.; Abed, A.M.; Safarova, L.; Jumanazarov, D.; Khudoynazarov, E.; Yadav, B.K.; Ben Khedher, N. Multiobjective Optimization of Double-Skin Façade Performance Using XGBoost and NSGA-II in Buildings Under Hot Climate Conditions. *Int. J. Energy Res.* **2026**, *2026*, 7007403. [CrossRef]
40. Congxiang, T.; Ahmad, N.A.; Abd Rased, A.N.N.W.; Hongchun, L.; Wenqing, L.; Abdalla, A.N. Parametric Multi-Objective Optimization of Rural Building Envelopes Using NSGA-II and Honeybee–EnergyPlus Simulation Framework. *Case Stud. Therm. Eng.* **2025**, *76*, 107297. [CrossRef]
41. Wang, A.; Xiao, Y.; Liu, C.; Zhao, Y.; Sun, S. Multi-objective optimization of building energy consumption and thermal comfort based on SVR-NSGA-II. *Case Stud. Therm. Eng.* **2024**, *63*, 105368. [CrossRef]
42. Tavares, G.G.; Ferraz, M.V.; Loureiro, E.V.; de Castro Nobre, V.; Goliatt, L.; Capriles, P. Thermal performance analysis of net-zero energy building using evolutionary algorithms. *Rev. Mundi Eng. Tecnol. E Gest. Ao (ISSN 2525-4782)* **2020**, *5* . [CrossRef]
43. Tavares, G.G.; Barbosa, S.; Goliatt, L.; Capriles, P. Airflow Analysis in a Double-Skin Façade Building Under Tropical Climates Using Evolutionary Algorithms. In *Proceedings of the International Congress on Information and Communication Technology*; Springer: Berlin/Heidelberg, Germany, 2023; pp. 309–318. [CrossRef]
44. Acosta-Medina, D.; Quintana-Gallardo, A.; Guillén-Guillamón, I.; Mediguchia, F.A. Evaluation of Passive Strategies for Achieving Hygrothermal Comfort in Social Housing Buildings in the Dominican Republic. *Sustainability* **2025**, *17*, 3416. [CrossRef]
45. CAIXA/IBGE. *SINAPI—Sistema Nacional de Pesquisa de Custos e Índices da Construção Civil*; Relatórios de Insumos e Composições; Caixa Econômica Federal, Brasília, DF, Brazil, 2025. Available online: https://www.caixa.gov.br/sinapi (accessed on 23 March 2026).
46. *ANSI/ASHRAE Standard 55-2023* ; Thermal Environmental Conditions for Human Occupancy. American Society of Heating, Refrigerating and Air-Conditioning Engineers: Peachtree Corners, Georgia, 2020.
47. *ISO 7730:2025*; Ergonomics of the Thermal Environment—Analytical Determination and Interpretation of Thermal Comfort Using Calculation of the PMV and PPD Indices and Local Thermal Comfort Criteria. International Organization for Standardization: Geneva, Switzerland, 2005.
48. Bernan, W. *History and Art of Warming and Ventilation of Rooms and Buildings*; Oxford University Press: London, UK, 1923.
49. Lin, C.y.; Zhang, Y. Combined effects of stress, depression, and emotion on thermal comfort: A case study in Shenzhen. *J. Build. Eng.* **2025**, *103*, 112158. [CrossRef]
50. Shang, W.; Liu, J.; Meng, H.; Jia, L.; Dai, X. A RL-based human behavior oriented optimal ventilation strategy for better energy efficiency and indoor air quality. *Energy Build.* **2025**, *345*, 116072. [CrossRef]
51. *ISO 7726:2025*; Ergonomics of the Thermal Environment—Instruments for Measuring Physical Quantities. International Organization for Standardization: Geneva, Switzerland, 1998.
52. *ISO 17772-1:2017*; Energy Performance of Buildings—Indoor Environmental Quality—Part 1: Indoor Environmental Input Parameters for the Design and Assessment of Energy Performance of Buildings. International Organization for Standardization: Geneva, Switzerland, 2017.
53. *EN 16798-1:2019*; Energy Performance of Buildings—Ventilation for Buildings—Part 1: Indoor Environmental Input Parameters for Design and Assessment of Energy Performance of Buildings. European Committee for Standardization: Brussels, Belgium, 2019.
54. *ABNT NBR 15575-1:2013*; Edificações Habitacionais—Desempenho—Parte 1: Requisitos Gerais. Associação Brasileira de Normas Técnicas: Rio de Janeiro, Brasil, 2021.
55. *ABNT NBR 15220*; Desempenho Térmico de Edificações. Associação Brasileira de Normas Técnicas: Rio de Janeiro, Brasil, 2005.
56. Ministério de Minas e Energia (MME). *PROJETEEE–Projetando Edificações Energeticamente Eficientes*; MME: Brasília, Brazil, 2025.
57. Associação Brasileira de Normas Técnicas. *NBR 15220: Desempenho Térmico de Edificações*; ABNT: Rio de Janeiro, Brasil, 2005.
58. Chitt, M.; Thangavel, S.; Kumar, A.; Singh, V.P.; Meena, C.S. Building performance prediction and optimization. In *Sustainable Technologies for Energy Efficient Buildings*; CRC Press: Boca Raton, FL, USA, 2024; pp. 241–257. [CrossRef]
59. Al Mindeel, T.; Spentzou, E.; Eftekhari, M. Energy, thermal comfort, and indoor air quality: Multi-objective optimization review. *Renew. Sustain. Energy Rev.* **2024**, *202*, 114682. [CrossRef]
60. Blank, J.; Deb, K. Pymoo: Multi-Objective Optimization in Python. *IEEE Access* **2020**, *8*, 89497–89509. [CrossRef]

61. Zamonato, B.; Faccin, H.; Grigoletti, G.d.C. Occupant behavior and energy consumption in residential buildings in a humid subtropical climate. *Ambiente Construído* **2025**, *25*, e148668. [CrossRef]
62. Balvedi, B.F.; Schaefer, A.; Bavaresco, M.V.; Eccel, J.V.; Ghisi, E. Identificação de perfis de comportamento do usuário para edificações residenciais multifamiliares e naturalmente ventiladas em Florianópolis. *Ambiente Construído* **2018**, *18*, 149–160. [CrossRef]
63. Ramos, G.; Lamberts, R.; Abrahão, K.C.; Bandeira, F.B.; Barbosa Teixeira, C.F.; Brito de Lima, M.; Broday, E.E.; Castro, A.P.; de Queiroz Leal, L.; De Vecchi, R.; et al. Adaptive behaviour and air conditioning use in Brazilian residential buildings. *Build. Res. Inf.* **2021**, *49*, 496–511. [CrossRef]
64. Dantas, L.G.; dos Santos, C.A.; Santos, C.A.; Martins, E.S.; Alves, L.M. Future changes in temperature and precipitation over northeastern Brazil by CMIP6 model. *Water* **2022**, *14*, 4118. [CrossRef]
65. Marengo, J.A.; Torres, R.R.; Alves, L.M. Drought in Northeast Brazil—past, present, and future. *Theor. Appl. Climatol.* **2017**, *129*, 1189–1200. [CrossRef]
66. Bottino, M.J.; Nobre, P.; Giarolla, E.; da Silva Junior, M.B.; Capistrano, V.B.; Malagutti, M.; Tamaoki, J.N.; de Oliveira, B.F.A.; Nobre, C.A. Amazon savannization and climate change are projected to increase dry season length and temperature extremes over Brazil. *Sci. Rep.* **2024**, *14*, 5131. [CrossRef]
67. Jeferson de Medeiros, F.; Prestrelo de Oliveira, C.; Avila Diaz, A.J. Evaluation of extreme precipitation climate indices and their projected changes for Brazil: From CMIP3 to CMIP6. *Weather Clim. Extrem.* **2022**, *38*, 100511 . [CrossRef]
68. Díaz-López, C.; Pérez-Rendon, C.A.; Serrano-Jiménez, A.; Barrios-Padura, A. Evaluating Resilience and Thermal Comfort in Mediterranean Dwellings: A Level(s) Framework Approach. *Appl. Sci.* **2025**, *15*, 2136. [CrossRef]

Disclaimer/Publisher's Note: The statements, opinions and data contained in all publications are solely those of the individual author(s) and contributor(s) and not of MDPI and/or the editor(s). MDPI and/or the editor(s) disclaim responsibility for any injury to people or property resulting from any ideas, methods, instructions or products referred to in the content.